5-1-2019

Potential Fossil Yield Classification (PFYC) Survey of Nevada Surficial Geology, and a Multi-Sensor, Remote Sensing, Change-Detection Study of Land-Use/Land-Cover Urbanization Impacting the Las Vegas Formation Located in Northwestern Las Vegas Valley

John Jayson Medema
geomedema81@gmail.com

A POTENTIAL FOSSIL YIELD CLASSIFICATION (PFYC) SURVEY OF NEVADA SURFICIAL GEOLOGY, AND A MULTI-SENSOR, REMOTE SENSING, CHANGE-DETECTION STUDY OF LAND-USE/LAND-COVER URBANIZATIONIMPACTING THE LAS VEGAS FORMATION LOCATED IN NORTHWESTERN LAS VEGAS VALLEY

By

John Jayson Medema

Bachelor of Science – Geology
University of Nevada, Las Vegas
2015

A thesis submitted in partial fulfillment
of the requirements for the

Master of Science –Geoscience

Department of Geoscience
College of Sciences
The Graduate College

University of Nevada, Las Vegas
May 2019

UNLV | GRADUATE COLLEGE

Thesis Approval

The Graduate College
The University of Nevada, Las Vegas

April 11, 2019

This thesis prepared by

John Jayson Medema

entitled

Potential Fossil Yield Classification (PFYC) Survey of Nevada Surficial Geology, and a Multi-Sensor, Remote Sensing, Change-Detection Study of Land-Use/Land-Cover Urbanization Impacting the Las Vegas Formation Located in Northwestern Las Vegas Valley

is approved in partial fulfillment of the requirements for the degree of

Master of Science –Geoscience
Department of Geoscience

Stephen Rowland, Ph.D.
Examination Committee Chair

Kathryn Hausbeck Korgan, Ph.D.
Graduate College Dean

Lynn Fenstermaker, Ph.D.
Examination Committee Member

Gabriel Judkins, Ph.D.
Examination Committee Member

Rebecca Martin, Ph.D.
Graduate College Faculty Representative

Abstract

This thesis is a combination of two separate but related projects. The first project is a Potential Fossil Yield Classification (PYFC) survey. The PFYC is a Bureau of Land Management funded survey designed to synthesize paleontologic information into a geographic information system (GIS) as a distributable geodatabase. The database is designed to represent surficial geologic deposits contained in a polygon shapefile. Throughout the State of Nevada each polygon represents a mapped geologic unit at a scale of at least 1:250 k. Each mapped geologic unit is then assigned a "potential fossil yield classification", a numerical ranking value of 1-5 based on the known fossils within a geologic unit. Fossil type and abundance are considered in the assignment of a PFYC value, 1 being the lowest, and 5 being the highest.

The second project consists of a multi-temporal land-use/land-cover change detection analysis designed to measure effects of rapid urbanization within a geologic unit identified to have the highest fossil potential based on the results of the PFYC survey. The Las Vegas Formation (LVfm) is a Pleistocene groundwater discharge deposit that has been shown to contain significant vertebrate fossils, thus being assigned a PFYC value of 5. The proximity of the LVfm to the densely populated city of Las Vegas provides a unique opportunity quantify effects of urbanization to lands rich with fossil resources. This project is designed to utilize remotely sensed imagery and aerial light detection and ranging (LiDAR) point clouds to accurately quantify urbanization effects

Table of Contents

List of Tables:

List of Figures

Chapter 1:

A Potential Fossil Yield Classification

Survey of Nevada Surficial Geology

Abstract

Paleontology has provided significant information about the history of life on Earth. Fossil floras and faunas are valued not only for their scientific properties, but also for their aesthetic and recreational values (Ligget, 2015). The information produced by a wide variety of geologic and paleontologic studies has yet to be synthesized into robust geodatabases for integration into a geographic information system (GIS) on a large scale. In recognition of this void, the Potential Fossil Yield Classification (PFYC) project was implemented by the Bureau of Land Management (BLM). PFYC is a numerical ranking system based on observed and documented information regarding the types and abundances of fossils contained within the spatial extent of a mapped geologic unit. PFYC rankings range from 1 to 5, with 1 indicating a very low potential fossil yield, and 5 indicating a very high potential fossil yield. A PFYC survey involves the collection, synthesis, and integration of paleontologic information into a geodatabase for ingestion and analysis in a GIS. Such a PFYC geodatabase is designed to allow land managers to more effectively identify, locate, plan for, and secure lands rich in fossil resources (Ligget, 2015).

In this project I inventoried and cataloged paleontologic information and knowledge from a wide array of sources into a single geodatabase. This geodatabase contains 2-D polygons representing all surficial geologic deposits at scales of 1:250k and 1:100k throughout the state of Nevada. One specific result of the Nevada PFYC project was the assignment of a PFYC level of 5 to Pleistocene groundwater discharge deposits associated with the Tule Springs Fossil Beds National Monument. These

deposits have been aggregated into the Las Vegas Formation (LVfm) (Longwell et al., 1965). The physical proximity of Tule Springs Fossil Beds National Monument to the cities of Las Vegas and North Las Vegas, along with significant population growth, has caused drastic land-use/land-cover change impacts to many of the mapped outcrops identified as the LVfm. These land-use/land-cover impacts illustrate the importance of a PFYC survey for allowing land managers to identify lands rich in fossil resources, as well as the value of organizing information geospatially to facilitate better management and protection of paleontological resources.

Introduction

Fossils provide significant information concerning the history of life. When an organism dies, if environmental and geological circumstances are favorable, the remains can be preserved indefinitely. This preservation provides a snapshot of life that includes information about the environmental and geologic conditions at the time of death. Take for instance a terrestrial vertebrate organism. The cause of death can vary widely, the key for preservation is hinged on the environment. The skeletal remains idealy need to be buried in some type of sediment. Once the skeletal remains are buried by sediment, on the scale of geologic time these sediments undergo lithification. During lithification the skeletal remains are re-mineralized as part of the lithified sediment.

Fossil resources have long been collected and studied in order to investigate how the Earth has changed over time. In 2009 the Paleontologic Resources Preservation Act (PRPA) was passed by Congress, providing sweeping regulations that introduced a standard inter-agency policy on how to manage fossil resources on federal

lands (https://www.blm.gov/programs/cultural-resources/paleontology). The regulatory statutes outlined in PRPA govern all lands managed by five separate federal agencies in the Department of Interior and Department of Agriculture. The BLM, one of these five agencies, has implemented a PFYC survey throughout multiple sates. The first objective in this study was to construct the PFYC geodatabase that meets all criteria in the BLM's standard scope of work for a PFYC survey.

In Nevada the federal government has legal control of more than 85% of land (Policy and Program Report, Research Division, Legislative Counsel Bureau 2016). The PFYC survey is intended to aid in determining which lands may need protection in terms of fossil resources, and which lands may be eligible for disposal, etc. Without the information contained in the PFYC survey, there is potential that lands rich in fossil resources will be transferred out of federal hands, thus jeopardizing the fossil resources and the intrinsic values they provide mankind. Additionally, the PFYC survey will enable the BLM to identify lands that may meet requirements for ownership transfer based on, for example, a very low PFYC assigned value. In addition to providing information related to fossil resources, the PFYC survey will capture a digital record of Nevada's surficial geology. Geologists acknowledge that the information contained in surficial geology is critical to investigating a variety of natural processes such as climate change (Rech et al., 2017). A particular surficial geologic unit identified to contain ancient shoreline features enable geologists to conclude the presence of past waterbodies. Nevada is located within the Basin and Range province and produces limited varieties of geologic units in terms of the abundances and distribution of vertebrate and invertebrate fossils as described in the PFYC survey results.

In 2014 Tule Springs Fossil Beds National Monument was established, effectively securing the remaining 22,650 acres of the upper Las Vegas wash and the groundwater discharge deposits identified as the Las Vegas Formation. The lands associated with this monument are rich in fossils from the late Pleistocene. Tule Springs Fossil Beds National Monument is administered by the National Park Service, one of the five agencies identified in the 2009 PRPA legislation. The PFYC survey classifies the surficial deposits of the Tule Springs Fossil Bed National Monument with the highest PFYC value. These deposits also occur in the area of Corn Creek Springs, approximately 30km northwest of the city of Las Vegas (Quade, 1985). Corn Creek Springs is managed by the Fish and Wildlife Service. Generally speaking, these fossil-rich groundwater discharge deposits lie in valleys that trend northwest-southeast. These valleys are flanked by alluvial fans emerging from both east and west sides of the valley (Quade, 1985). Las Vegas Valley is a product of Neogene extension that formed the Basin and Range Province of western North America (Springer et al., 2017). This Neogene extension is related to the activity of tectonic plates along the western continental boundary of the North American Plate. As the Pacific Plate began to subduct beneath the North American Plate two triple plate junctions were create. One at the intersection of the Pacific, Juan De Fluca and North American Plates, the second between the Pacific Cocos, and North American Plates. The corresponding vector mechanics between the Pacific and North American Plates created a transform boundary, which as a result of this transform boundary the San Andreas Fault zone was formed. This massive transform boundary is understood as a driving mechanism in the Neogene extension of Nevada.

The sediments associated with and located within Tule Springs Fossil Beds National Monument have been yielding vertebrate fossils for over 100 years. The area first generated significant scientific attention with the discovery in 1933 of an obsidian flake and associated bones of extinct Pleistocene animals (Rowland and Bonde, 2015). These strata were extensively investigated in 1962-63 (Nevada State Museum ref. 1967). The Las Vegas Formation was originally defined by Longwell et al. (1965); Haynes (1967) subdivided it into members A-G. The fossils collected, include a diverse Rancholabrean-age, Late Pleistocene fauna, including but not limited to giant camel, Columbian mammoth, bison, horse, dire wolf and American lion (Springer et al., 2017). An underlying objective of the PFYC project is to capture these paleontological data and integrate them into a database.

To accomplish the objectives of this PFYC survey I have followed a standard scope of work designed by the BLM (Appendix A). I produced two layers contained in a geodatabase: a geology layer and a map layer. The layers are contained inside ESRI's (Environmental Systems Research Institute) ArcGIS, which is recognized as the industry leader in GIS.

A layer is simply a reference to a specific object or feature and all of the properties associated with it (Longley et al., 2015). The PFYC geology layer is a polygon shapefile that contains all surficial geological units for the State of Nevada at scales of 1:250k and 1:100k. The PFYC map layer is also a polygon shapefile that provides a visualization of the spatial distribution representing the allocated geologic maps used to generate the geologic polygons. Each layer contains a table; the attribute fields and organizational parameters are provided in detail in Appendix A.

Detailed information regarding the fossil resources contained within particular geologic units occur in a multitude of papers and geologic map reports. For Nevada's PFYC survey a supplemental paper will be published. This paper will provide all referenced literature used in assigning a PFYC value to geologic units. The PFYC project provides a robust data product that queries these sources for specific paleontologic information and synthesizes the desired information into a single geodatabase for analysis in a geographic information system (GIS). The types of data that can be ingested into a particular GIS drastically increased in the latter half of the 20th century, and this trend continues in the 21st century (Longley et al., 2015). As our world continues to develop in a digital sense it is important to understand that a vast majority of information that is generated on a daily basis contains spatial information, and as we continue to create these data the entire world is moving forward, effectively becoming an interconnected GIS (Longley, et al., 2015). Modern paleontology is beginning to utilize GPS by capturing GPS coordinates of valuable fossils, this integration of geospatial information with paleontology can be easily ingested into a particular states PFYC geodatabase.

Methodology

The BLM provided a standard scope of work document designed as an architectural foundation from which to produce the two layers existing inside the PFYC geodatabase. The two layers are identified as the geology layer and the map layer. The geology layer is a polygon shapefile representing surficial geology throughout the boundary of the state of Nevada at a minimal scale requirement of 1:100k. The map

layer is a second polygon shapefile designed to be an annotated visual representation identifying all geologic maps, and their respective spatial boundaries, used to generate the geology layer.

The first iteration of the geology layer was derived from a USGS polygon shapefile representing surficial geology at a scale of 1:500k. This scale did not meet the requirements outlined in the standard scope of work and thus was discarded. The Nevada Bureau of Mines and Geology (NBMG) provided a database containing geology polygon shapefiles. The NBMG product was the result of digitizing all Nevada county maps at a scale of 1:250k, producing 15 individual polygon shapefiles representing geologic polygons derived from the published county maps. The NBMG donated copies of the databases for this project. These 15 shapefiles were merged together into a single shapefile. This new shapefile was used as a new base map, representing all surficial geology at larger scale of 1:250k projected into North American Datum (NAD) 1983 in UTM zone 11N. This base map will be referred to as the NBMG base map.

The corresponding geologic map survey was conducted through the USGS National Geologic Map Database (NGMDB) https://ngmdb.usgs.gov/ and the Nevada Bureau of Mines and Geology (NBMG) geologic map database http://www.nbmg.unr.edu/Maps&Data/. I surveyed these resources to locate all geologic maps within the State of Nevada at the 1:100k scale for digitizing. Three of the published 1:100k maps focused primarily on Quaternary geology. Subsequent research was conducted to investigate whether the mapped Quaternary units contained significant fossil resources. This inquiry did not identify any mapped Quaternary units that contain significant fossil resources, thus these maps were not used for manual

digitizing purposes. A total of five geologic maps at 1:100k scale were available for digitizing, and a single 1:120K scale map representing the Nevada National Security Site (N2S2), formerly the Nevada Test Site (NTS), were allocated. Additionally, there are three maps at the 1:100k scale that are in the process of being published; due to the time constraints of the PFYC project these maps were not used. A detailed list of all geologic maps used in the construction of the geology layer is provided in Appendix B.

The next step for the geology layer was to integrate the larger scale 1:100k geologic map information into the smaller scale NBMG base map. I achieved this by extracting the surficial geology from the digital geologic maps and digitizing those data accurately into polygons representing the actual mapped geology. I developed a methodology that I termed “cut-in” digitizing which involved downloading the digital geologic maps as tagged image files (.tif or.tiff). A .tiff can be an image file that contains geospatial reference information. I then intersected each geologic map, one by one, with, the NBMG base map, and I traced the spatial extent using a single polygon. This polygon defined the area and spatial extent of coverage provided by the 1:100k maps. I then used this polygon to ‘cut out’ or clip out the area within the NBMG base

map,creating a void of information to be filled in by digitizing new polygons derived from the 1:100k geologic map (*Fig. 1*).

I generated the new polygons representing the mapped geology contained in the 1:100k geologic map by manually digitizing, tracing by hand each individual geologic unit from the digital map defined throughout the map extent (figures 2 & 3). To ensure spatial consistency between adjacent digitized geologic polygons, the ‘autocomplete polygon’ was the standard mode used to create all polygon features within the shapefile. Once completed I symbolized all digitized geologic units with graduated color ramp that is structured on each individual geologic units PFYC coded values. The Map Layer was also created through digitizing polygons. I traced each geologic map

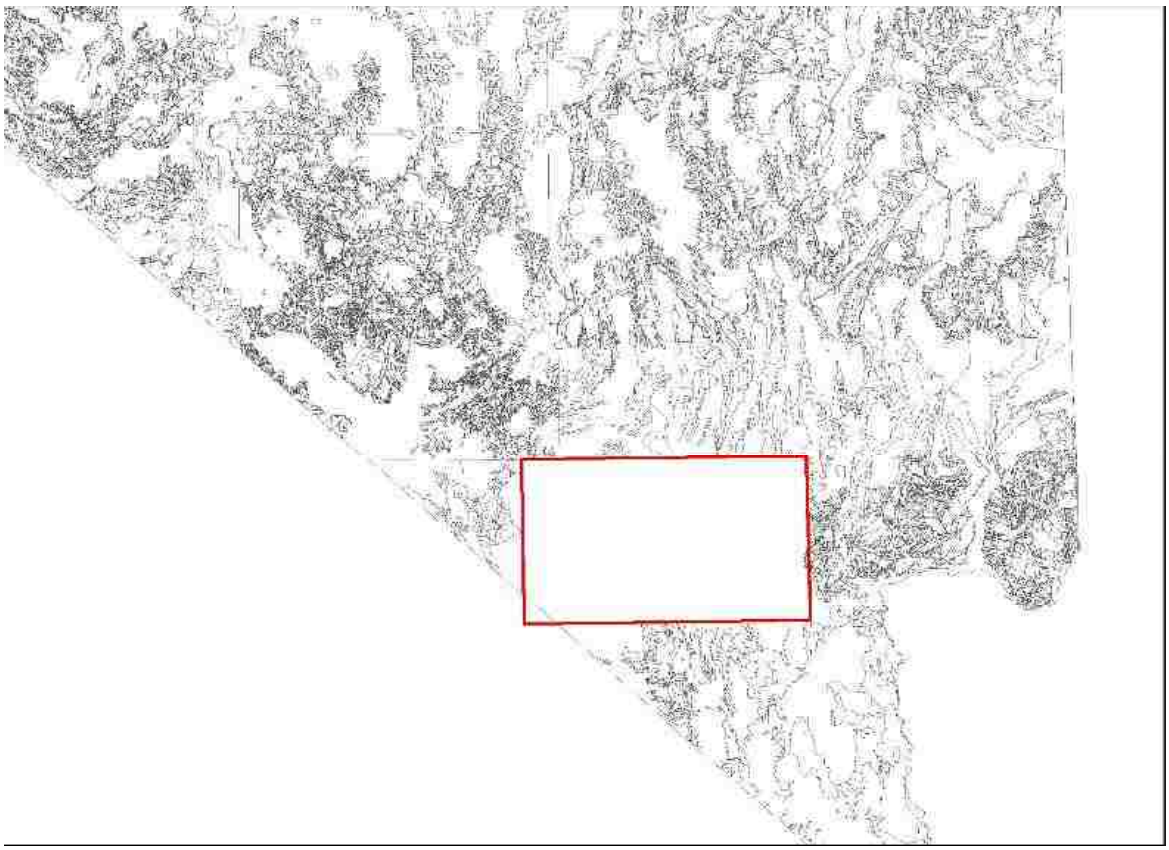

Figure 1:'Cut-in' digitizing result. Polygons from the NBMG base map layer were extracted/deleted using the boundary of the Las Vegas 30x60 quadrangle. Creating the window to manually trace geology, digitizing new polygons at the larger scale of 1:100k

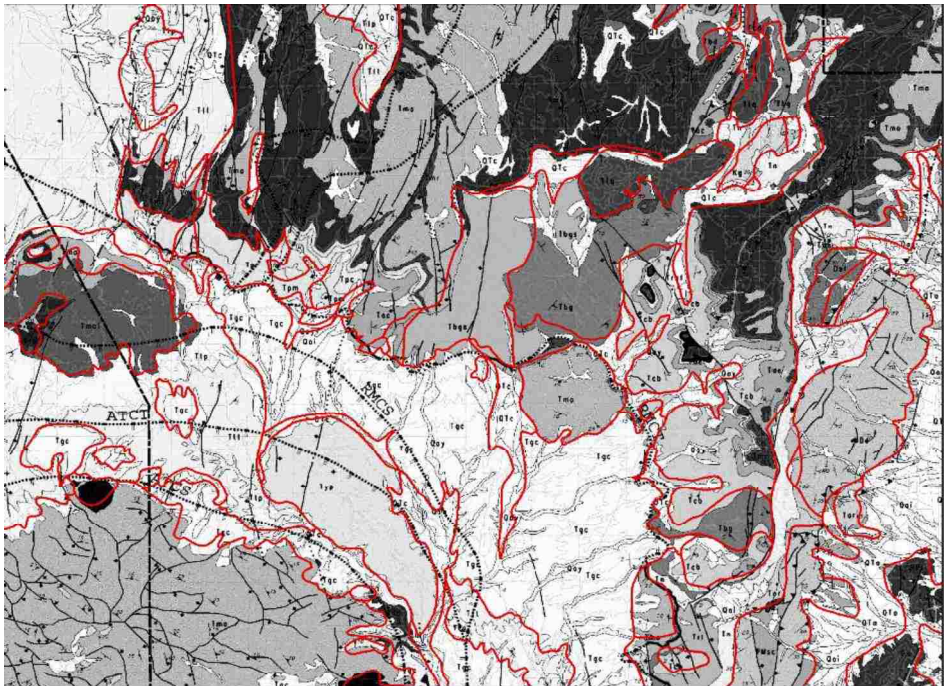

Figure 2: Red lines represent the manual digitizing efforts. The new digitized polygons accurately represent geology as mapped in the Digital geologic map of the Nevada Test Site and vicinity, Nye, Lincoln, and Clark Counties, Nevada, and Inyo County, California.

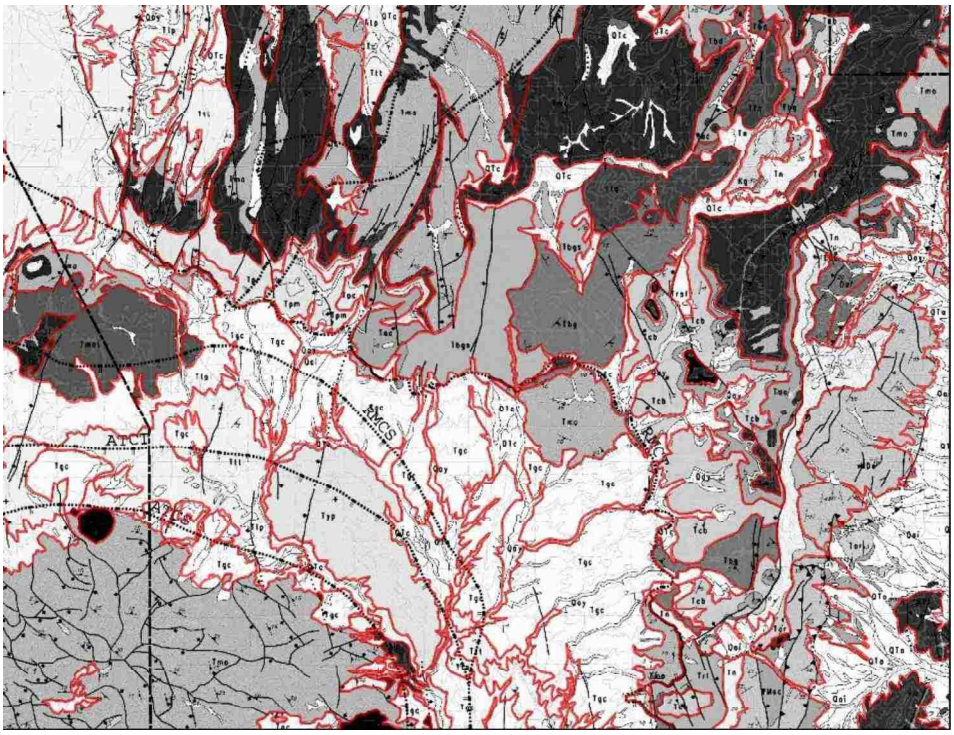

Figure 3: Red lines represent the NBMG base map geologic polygons. These are intersected with the larger scale geologic map titled Digital geologic map of the Nevada Test Site and vicinity, Nye, Lincoln, and Clark Counties, Nevada, and Inyo County, California.

boundary to identify the spatial extent of its coverage. The construction started with the 15 county maps; the counties of Lyon, Douglas, and Carson were all merged together into a single shapefile. A comprehensive list of all geologic maps used for digitizing is listed in *table 1*. I then traced and integrated the remaining larger scale geologic map boundaries integrated them into the map layer. The map layer holds its own attribute table, populated with relevant fields and domain values, as per the BLM standard scope of work.

Results

Most geologic units within the state are assigned PFYC values of 1, 2 and 3. A robust distribution of PFYC values of 1 includes igneous, metamorphic and volcanic rocks. Most of the Quaternary units are assigned PFYC values of 2; very few Quaternary units have been assigned higher values. The spatial distribution of PFYC values 1, 2, and 3 correspond with Basin and Range geology and can easily be distinguished in the final geology layer map (*Fig. 4*). Significant exposures of Paleozoic sedimentary marine units with invertebrate fossils are generally classified with a PFYC value of 3, however the PFYC survey did identify Paleozoic marine units with higher PFYC classifications. For example, the Deep Spring Formation in Esmeralda County, which straddles the Ediacaran-Cambrian boundary, is assigned a PFYC value of 4 because of documented preservation of stromatolitiic reefs as well as scientifically significant metazoan and algal fossils (Rowland, et al., 2008). The Poleta Fm, a Cambrian sedimentary marine unit, has been documented to contain Lägerstatten-quality preservation of invertebrate soft-bodied organisms similar to the Burgess Shale Lagerstätte (English and Babcock, 2010). The Devil's Gate Limestone, a Devonian marine carbonate unit was assigned a PFYC value of 4, due to the recorded preservation of fish and basal tetrapods (Murphey et al., 1976; Swartz, 2012).

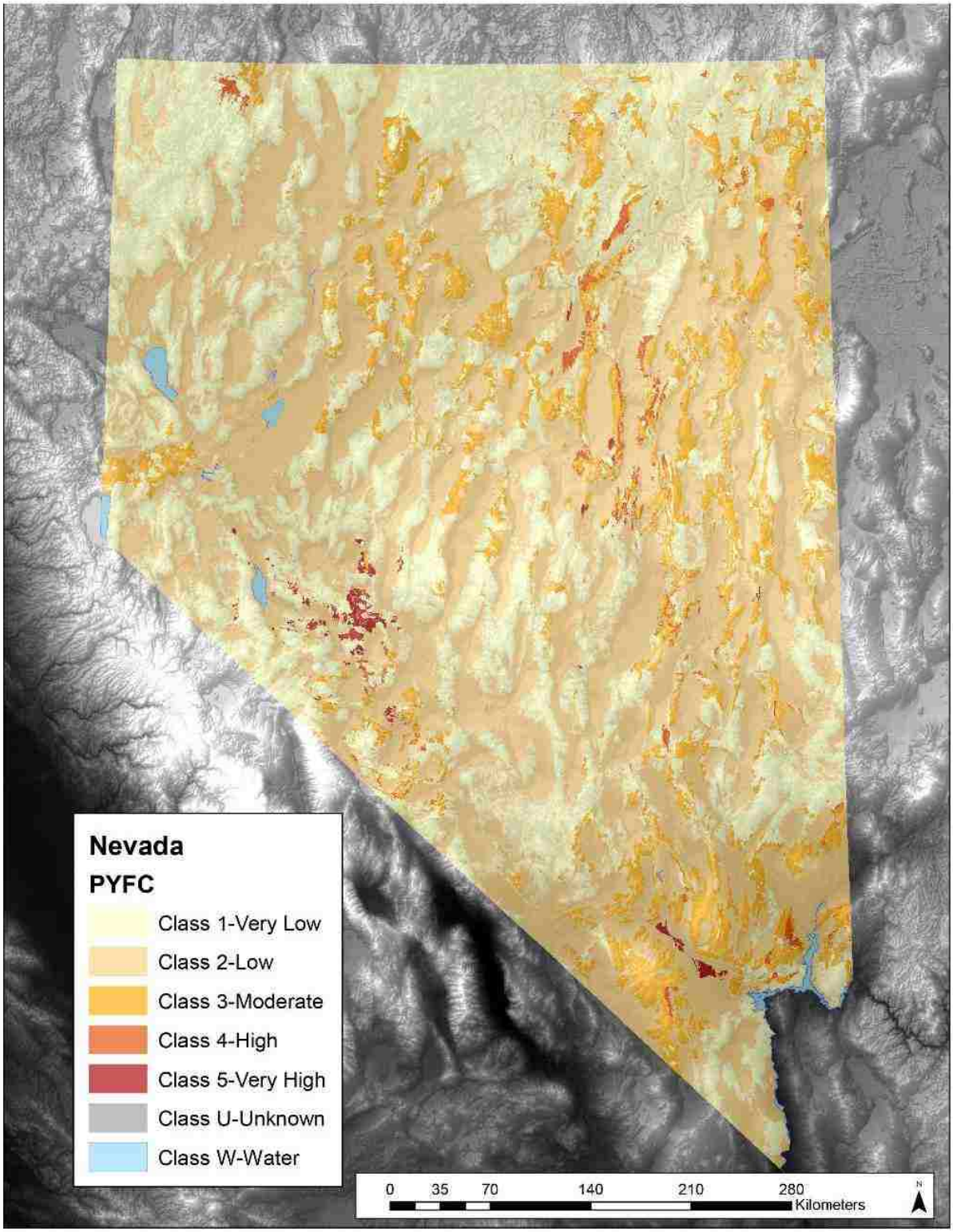

Figure 4: Completed Nevada PFYC survey geology layer

Very few units are identified as having a very high potential fossil yield or (PFYC value of 5). Two units that have been assigned this value are the Newark Canyon and Willow Tank Formations. The Newark Canyon Formation is a Cretaceous unit exposed in Eureka County. It consists of lacustrine sediments, as well as deposits derived from a wedge-top basin, and it contains invertebrate fossils and terrestrial vertebrate fossils (MacNeil, 1939; David, 1941; Bonde et al., 2015). The Willow Tank Formation, exposed in eastern Clark County, is also a Cretaceous terrestrial unit. It has produced significant terrestrial vertebrate and plant fossils (Bonde et al., 2008, 2012).

The two most significant units assigned a PFYC value of 5 are the Esmeralda Formation, located along the eastern boundaries of Esmeralda and Mineral counties, and the Las Vegas Formation located in Clark County. The Esmeralda Formation consists of volcaniclastic, lacustrine, and fluvial units. This Miocene formation has been documented to contain significant plant macrofossils and terrestrial vertebrate fossils (Hardy and Bonde, 2015; Hardy and Humphrey, 2018). In Paleontology there is a succinct distinction between invertebrate, vertebrate and plant fossils. Vertebrate fossils, if present are awarded higher PFYC values.

In Nevada, there are several significant units assigned a PFYC value of 4, such as the Favrer Formation and the Aztec Sandstone. The Favrer Formation consists of Triassic marine carbonate deposits containing abundant invertebrates and some marine vertebrate fossils (Hopkin and McRoberts, 2005). Prior to 2012 the Aztec Sandstone was not known as a fossiliferous unit. Since 2012 the Aztec Sandstone has produced trace fossils in Valley of Fire State Park and Red Rock Canyon National Conservation Area. (Stoller et al., 2013; Rowland et al., 2014). The fossil trackways in the Aztec

Sandstone have been studied in detail and are believed to represent tritylodontid therapsids, small herbivorous synapsids (Rowland and Mercadante, 2014) as well as Theropod dinosaurs and multiple taxa of arthropods (Rowland et al., 2014).

Several Paleogene and Neogene units have been assigned a PFYC value of 4 and one Paleogene unit, the Sheep Pass Formation, was assigned a PFYC value of 5. The Quaternary has produced a single unit assigned a PFYC value of 5, the Las Vegas Formation. The Las Vegas Formation consists of Pleistocene groundwater discharge deposits and contains significant Ice-Age megafauna fossils (Springer et al., 2017). The units located in the upper Las Vegas Wash that I have integrated into the Las Vegas Formation are known to contain the largest Rancholabrean vertebrate fossil assemblage currently known in the Mojave Desert region (Scott et al., 2017). A complete list of all the members of the Las Vegas Formation and laterally equivalent units is provided in Appendix C.

The final geology layer (*Fig. 4*) consists of 36,797 individual polygons representing surficial geology within the boundary of the State of Nevada. The corresponding attribute table for the geology layer, with all fields and records satisfying the BLM's standard scope of work, contains 883,128 records. The 'cut-in' digitizing of all allocated 1:100k-scale geologic maps significantly increased the total amount of digitized polygons. This increase was a function of scale related to geologic mapping. At the smaller scale, a specific geologic unit may be identified and mapped. On a larger scale that same geologic unit is often differentiated into two or more separate units, often differentiating separate members of a formation. The BLM scale standard for any given states PFYC survey states that the polygons should represent geology at the

scale of 1:100k. This scale standard provides significantly more detail than a scale of 1:250k. This higher level of detail provides a generalized distinction between geologic units that may or may not contain fossil resources as a generalized reference at the scale of 1:100k.

The second, and final deliverable was the geologic map layer (*Fig. 5*). The function of this deliverable is designed as a visual representation of all geologic maps used in the construction of the geology layer. The geologic map layer also contains its own table architecture that is also outlined in the BLM standard scope of work.

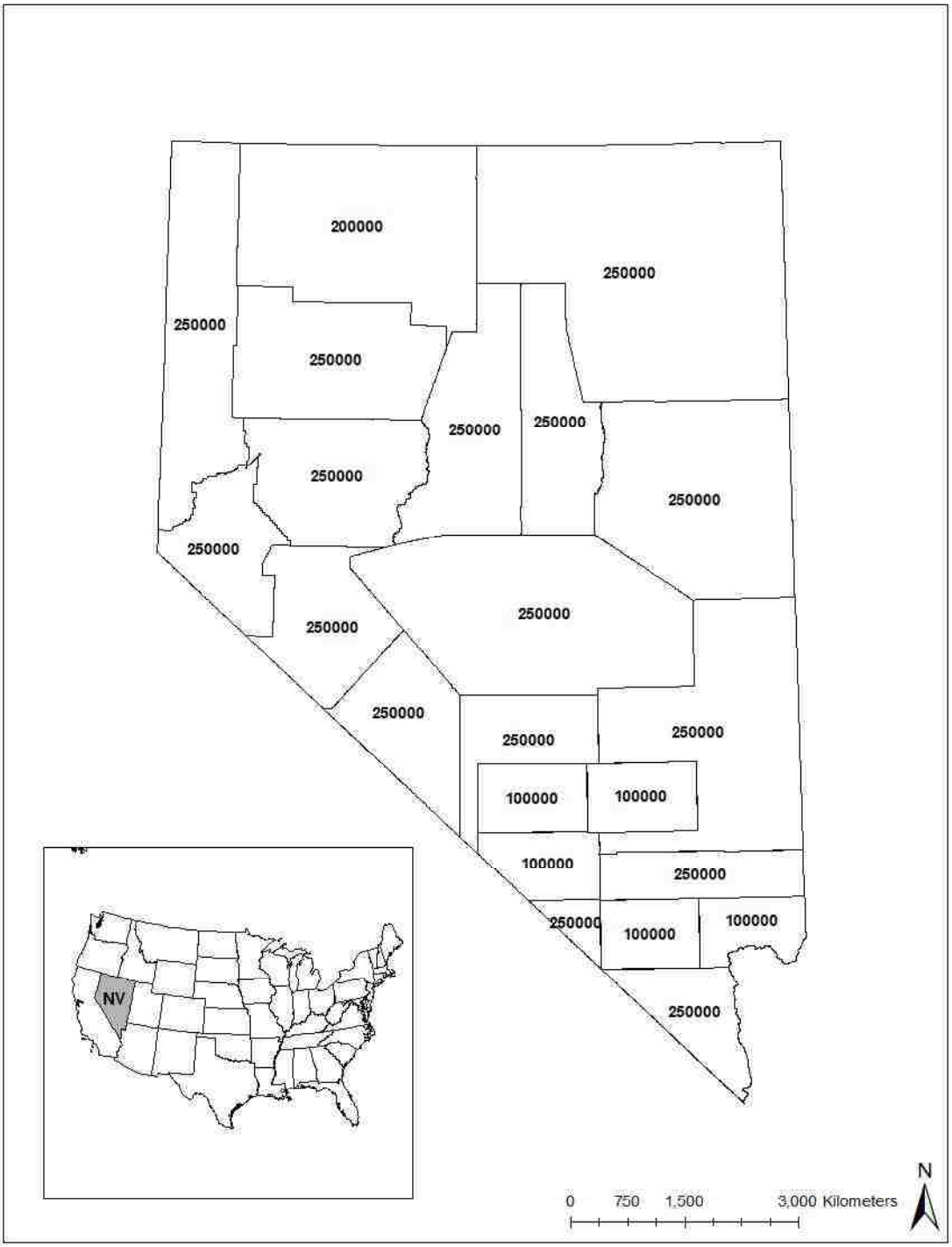

Figure 5: Map layer representing the scale and extent of all geologic maps used to digitize geologic polygons

Discussion

The goal of the PFYC survey was to identify lands containing valuable fossil resources and classify them on a scale of 1 to 5. The PFYC geology layer results suggest that the initial scale limitations be re-evaluated. The scale standard established by the BLM for the PFYC project proved to be problematic for this survey. My review of the literature used to justify assigning PFYC values identified many geologic units to which I assigned PFYC values of three or higher. However, some of these units are not included in the Nevada PFYC geodatabase because the units do not appear at the 1:100 k scale. Many of these fossiliferous units are only identified and mapped at a scale of 1:24 k. Because of this scale-based phenomenon, I recommend that the scale limit be re-evaluated on a case-by-case basis. If, as I have observed in portions of Nevada, there are outcrops of fossiliferous units that qualify for designation with a high PFYC value, then the area containing those units should be mapped at a large enough scale to differentiate them from the surrounding geology. Accommodation of these units at larger scales would produce a more complete and robust representation of identified fossil resources. Accommodation of larger-scale-based digitizing would significantly increase the total amount of digitized polygons in the geodatabase, but a more robust and complete data set would be created.

A good example of this problem is the Neogene Buffalo Canyon Formation, exposed in Churchill County. This formation has produced a significant fossil flora and fauna. (Stidham & Stidham, 2000) This literature justified assigning the Buffalo Canyon Formation a PFYC Value of 4. However, due to the scale parameters set by the BLM

this formation is not contained within the geology layer of the PFYC geodatabase. The geologic polygons in the area of eastern Churchill County are derived from the 1:250k digital geologic map of Churchill County. All geologic polygons are assigned a PFYC value according to the unit descriptions provided in the respective geologic map used to digitize the polygon. In the case of the Churchill County map, the geology in the area containing the Buffalo Canyon formation is described to be older sedimentary rocks, surrounded by volcanic lithologies. Thus, at the scale the geologic polygon is digitized, in this case 1:250k, it is assigned the PFYC value according to the unit's description.

The Las Vegas Formation, assigned the highest PFYC value of 5, was captured by the 1:100 k scale geologic maps. The Las Vegas Formation, portions of which are protected within Tule Springs Fossil Beds National Monument, and Ice Age Fossils State Sark, has experienced significant impacts due to land-use/land-cover change. If a PFYC survey or similar investigation had been conducted prior to the surge in population growth rates in Las Vegas Valley in the late 1990's through 2005 (Kotz, 2009) additional portions of the fossiliferous Las Vegas Formation could have been protected and significant land-use/land-cover impacts averted, preserving these fossil-rich areas for future study. The loss of area within The Las Vegas Formation illustrates the value of a PFYC survey. Such a survey not only identifies of lands rich in fossils, it also empowers land managers to make better planning choices based on identifiable characteristics other than proximity to the developing fringe of the Las Vegas Metropolitan region.

The map layer that accompanies the geology layer in this study is a visual representation of the extent and distribution of all geologic maps used to generate

digitized geologic polygons. The initial survey conducted to identify relevant geologic maps indicated that the state of Nevada has very limited coverage of 1:100 k scale maps. In comparison, the PFYC survey conducted for Montana and the Dakotas by Ligget (2015) has far more complete geologic map coverage at the 1:100 k scale. The map layer for Ligget's PFYC survey showed that the entire state of Montana had complete coverage of geologic maps at 1:100 k scale. The lack of consistent 1:100 k scale geologic map coverage illustrates the sparse availability throughout the State of Nevada. In addition to the sparsity of 1:100 k scale geologic maps, the detailed Tule Springs study illustrated additional sparsity in 1:24 k scale geologic map coverage in southern Nevada. These information gaps should be further investigated, and efforts should be made to reduce them. This data gap exposed by the Nevada PFYC survey should provide sufficient justification for the investment of resources to address this data gap in Nevada. Once the data gap is addressed an effort should be made to re-evaluate the Nevada PFYC geologic unit layer to produce a more consistent geologic layer in terms of the scale of the polygons contained in the PFYC Geologic Unit layer.

Chapter 2:

A Multi-Temporal Land-use/Land-cover Impact Assessment of the Las Vegas Formation

Abstract

This project examines multi-temporal impacts of land-use/land-cover changes within a geologic formation assigned a class 5 (very high) fossil potential value through a Potential Fossil Yield Classification (PFYC) survey. Best known from exposures in northwestern Las Vegas Valley, the Las Vegas Formation (LVfm), has experienced significant impacts due to rapid urbanization. The physical proximity of the LVfm to the cities of Las Vegas and North Las Vegas, along with significant population growth, has resulted in dramatic land-use/land-cover changes to many of the outcrops. These land-use/land-cover impacts illustrate the importance of a PFYC survey for allowing land managers to identify lands rich in fossil resources, as well as the value of organizing information geospatially to facilitate better management and protection of paleontological resources.

Satellite-based, remote sensing and image analysis has enabled researchers to accurately monitor physical changes in Earth's surface over time. In this study I utilized both multisensor feature classification and multi-temporal change detection methods. The multi-sensor feature classification is executed by the combination of aerial light detection and ranging (LiDAR) point clouds, and high-resolution aerial imagery acquired via the National Agriculture Imagery Program (NAIP). Multi-temporal, change-detection methodology was evaluated by investigating the physical properties to sparsely vegetated, fine-grained deposits representing the LVfm. The results of this study indicate that the short-wave infrared bandwidths calibrated to radiance, top of atmosphere reflectance and a "brightness" image derived from Tasseled Cap

Transformation are most effective in accurately quantifying changes to the surface of the LVfm over time. Preliminary evaluations indicated that these image types yield less than 10% difference in area when compared with the area calculated from the LiDAR. These data presented in this project suggest for multi-temporal studies conducted in arid environments, and for surfaces with similar physical characteristics, the results provide high levels of accuracy

Introduction

The objective of this study was to use a remote-sensing, change-detection technique to analyze rapid urbanization in the greater Las Vegas area, specifically in and around Tule Springs Fossil Beds National Monument. Change-detection methods have been widely studied and practiced, providing confidence in the ability to use remote sensing to provide geospatial data for urban land-use/land-cover mapping and for monitoring environmental changes (Zhang et al., 2002). Change detection begins with the observation and identification of an object, in this case a geologic surface, and monitoring it over time (Singh et al., 1989).

To execute this multi-temporal analysis, I utilized a combination of remotely sensed satellite imagery and aerial light detection and ranging (LiDAR) for accuracy evaluation. Digital satellite image products have been used by many remote sensing researchers to quantify and classify environmental changes, such as changes in forest canopy areas, desertification of lands as well as urbanization (Singh et Al 1989). Recently LiDAR data have been integrated with multispectral aerial and satellite imagery to improve land-cover classification (Im et al., 2008), a method that I

implemented for this study. I used the results of the remote-sensing, change-detection analysis to quantify land-use/land-cover impact within the defined boundary of the LVfm. Additionally, I distributed these results over a temporal range, which allows me to provide additional commentary concerning the correlation of the land-use/land-cover impacts and population growth in the Las Vegas area.

Remote sensing provides robust, large-scale, multi-temporal image products that allow land-cover information to be quantitatively measured (Mas et al., 1999). For this study I selected the Landsat satellite sensor because of the longevity in terms of temporal record. The Landsat satellite sensor provides the longest record of satellite imagery products. In 1972 the first sensor was launched under the name Earth Resources Technology Satellite, later renamed Landsat 1. Continuing Landsat sensors have been launched since the late 70's with Landsat 9 expected to launch in 2020. The Landsat satellites have been proven a valuable source of data for monitoring changes on the Earth's surface (Markham et al., 2009). Landsat is a joint operations project between the USGS and the National Aeronautics and Space Agency (NASA). I acquired Landsat Sensors 5 and Landsat 8 Operational Land Imager (OLI). Landsat 5 Thematic Mapper (TM) operated from 1984 to 2011; it provides a 7-band, multi-spectral-image product with 30 m spatial resolution. This includes three bands in the visible range of 0.45-0.69 microns, as well as two near infrared (NIR) bands and two shortwave infrared bands (SWIR), also at 30m per pixel. The Landsat 8 OLI sensor, which was launched in 2013, provides the same spatial resolution across the visible, NIR, and SWIR spectral ranges, and also includes two thermal-infrared-band-sampling, as well as a ninth band called Cirrus. The Landsat 8 OLI sensor SWIR bandwidths were recalibrated to record

samples in Band 6 at 1.57 μm -1.65μm and Band 7 at 2.11μm -2.29μm from previous Landsat sensors. Previous Landsat Thematic Mapper sensors recorded SWIR wavelengths at a wider range in Band 5 at 1.55μm-1.75μm and Band 7 in 2.08μm-2.35μm.

The United States Geological Survey (USGS) hosts a significant collection of remotely sensed image products that are available from the data portal EarthExplorer, https://earthexplorer.usgs.gov/. I queried this data portal to obtain all imagery used for analysis in this project. Each multi-temporal Landsat scene was acquired at Landsat Level 1 standard, where each pixel value represents calibrated digital numbers (DN).

The LiDAR product was also acquired through EarthExplorer; I downloaded these LiDAR datasets as a log ascii standard (.las) file which is the most common method for using LiDAR products. Airborne LiDAR accurately records and identifies ground features at sub-meter accuracies (Crutchley, 2006). LiDAR measures the time it takes a pulse of light to reach a target and return. Modern LiDAR sensors produce a very dense scan of objects and return high-resolution point-cloud models of the features scanned (Crutchley, 2006). The resulting point clouds offer 3-dimensional data products that have the ability to be post-processed manually or though automated script-based algorithms which can assign point classifications, such as classification of a point based on its height (z value). Integration of multi-sensor data has become popular for applications directed at the classification of surface objects using remotely sensed data (Yan et al 2015). This method combines high-resolution imagery with the LiDAR and has yielded promising results in terms of land-cover classifications. However, high accuracy can be obtained only if two critical criteria are met: (1) the data

must be registered in the same coordinate system, and (2) the spatial resolution of each dataset must be identical or matched (Yan et al., 2015.) In 2010 the Southern Nevada Water Authority (SNWA) collected aerial LiDAR data for Las Vegas Valley. The SNWA LiDAR data were allocated and processed to generate a "ground truth" measure of land-use/land-cover change. I used the "ground truth" measurement to identify the most accurate method of change detection by comparing the results of each iteration of change detection on all 2010 image types to the 2010 LiDAR "ground truth".

Methodology

(Pt. 1 Refining Las Vegas Formation Boundary for Larger Scale)

The LVfm was assigned a PFYC value of 5 in accordance with the BLM. The scale parameters for the PFYC project outlined by the BLM, required all digitized polygons to represent mapped geology at scales too small to effectively represent the LVfm at the level of detail I wanted for this project. The first boundary identified as the LVfm and all Pleistocene groundwater discharge deposits was derived from geologic maps at a scale of 1:100k. I investigated this boundary with the goal of generating the most accurate spatial representation of the LVfm groundwater discharge deposits. I began this boundary investigation with a re-assessment of the LVfm units with respect to larger scale geologic map information. I then searched for geologic maps of the northwestern Las Vegas Valley, Upper Las Vegas Wash area. I reviewed these maps to identify units associated with late Pleistocene groundwater discharge deposits. I then re-digitized, using the same manual digitizing techniques implemented in the initial construction of the PFYC geology layer, as described in Chapter 1. This query yielded

four geologic maps at a scale of 1:24k, listed in *Table 2*. These are the only geologic maps that contain detailed unit descriptions that include Pleistocene groundwater discharge sediments in the Upper Las Vegas Wash area.

Table 1: List of Geologic Maps used to re-define boundary of the LVfm

TITLE	Scale	Publication Year
Geologic Map of the Corn Creek Springs Quadrangle, Nevada	1:24000	1999
Geologic Map of the Gass Peak SW quadrangle, Clark County, Nevada	1:24000	2009
Tule Springs Park Quadrangle, Nevada	1:24000	1998
Preliminary geologic map of the Valley qundrangle, Clark County Nevda	1:24000	1998

The LVfm boundary derived from the 1:100k scale survey (Fig 6.) compared to the larger scale derived LVfm boundary (*Fig. 7.)* shows a significant decrease in total area and a greater distribution of total polygons defined as the LVfm, most units of which are associated with Pleistocene groundwater discharge. The hard edge border in the south-east and southern edges is a function of the unit descriptions contained in The Valley Quadrangle, Las Vegas NE and NW quadrangle maps. These maps do not specify any Pleistocene GW discharge deposits; therefore, I did not include any of the mapped geologic units from the aforementioned published maps. The final shape derived from the 1:24k geologic maps has a smaller total area and is identified as the most accurate boundary identifying the extent of the LVfm. This new larger scale boundary represents all geology containing unit descriptions fitting the definition of the Las Vegas Formation, containing Pleistocene ground-water discharge sediments. The area that is identified as the Las Vegas Formation boundary is a derivation of a digital

geologic map, and it is acknowledged that there is a possibility that the sediments contained within this boundary can undergo physical erosion via fluvial or aeolian mechanisms effectively transporting weathered out fossil remains outside of this boundary.

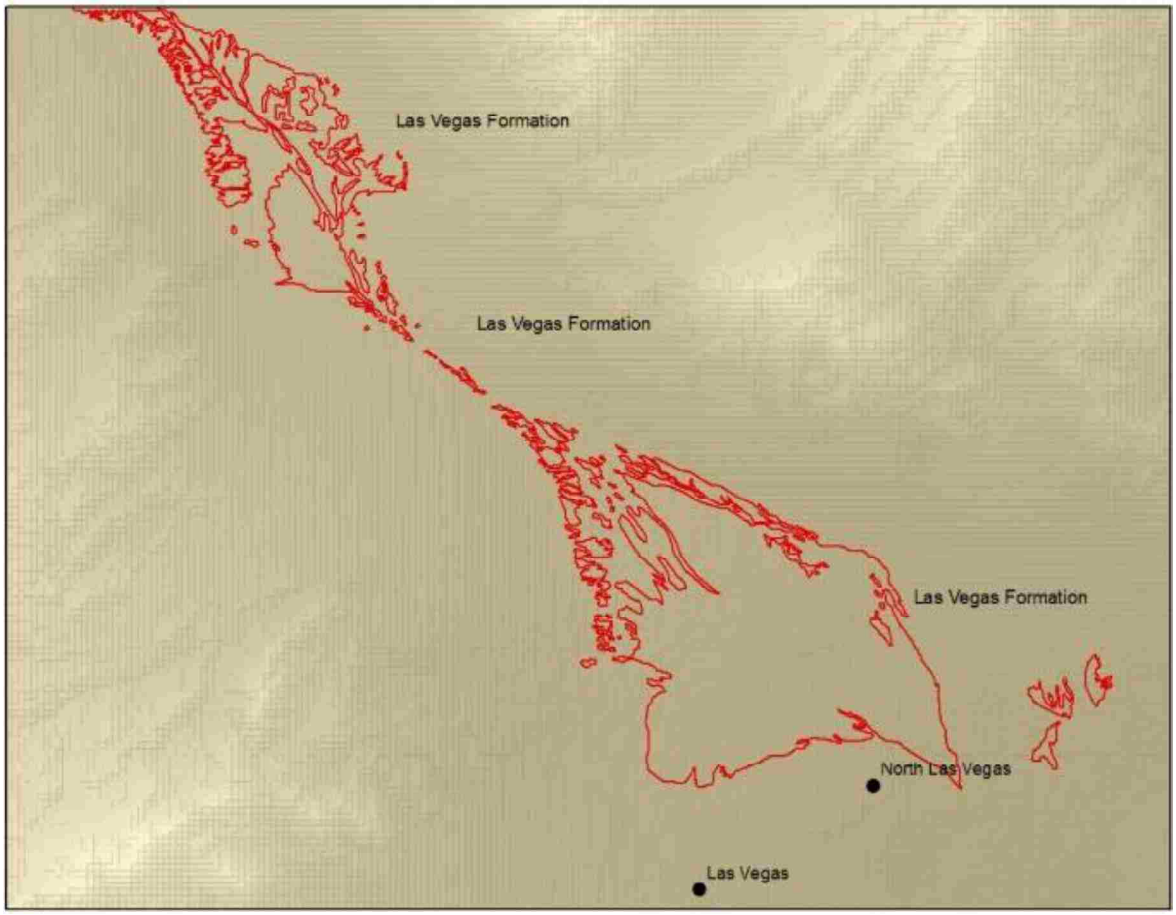

Figure 6: The Las Vegas Formation boundary as derived from 1:100k scale geologic map data.

The new larger scale boundary is identified as the Las Vegas Formation and consists of only late Pleistocene groundwater discharge deposits based on the unit descriptions provided with each published map. This area is the area of interest (AOI)

for the quantitative land-use/land-cover impact analysis. A complete list of all Pleistocene groundwater discharge units selected and digitized, including the detailed unit descriptions, provided in Appendix C. The new 1:24k scale boundary was ingested into ESRI ArcMap software, and the area of this boundary was calculated.

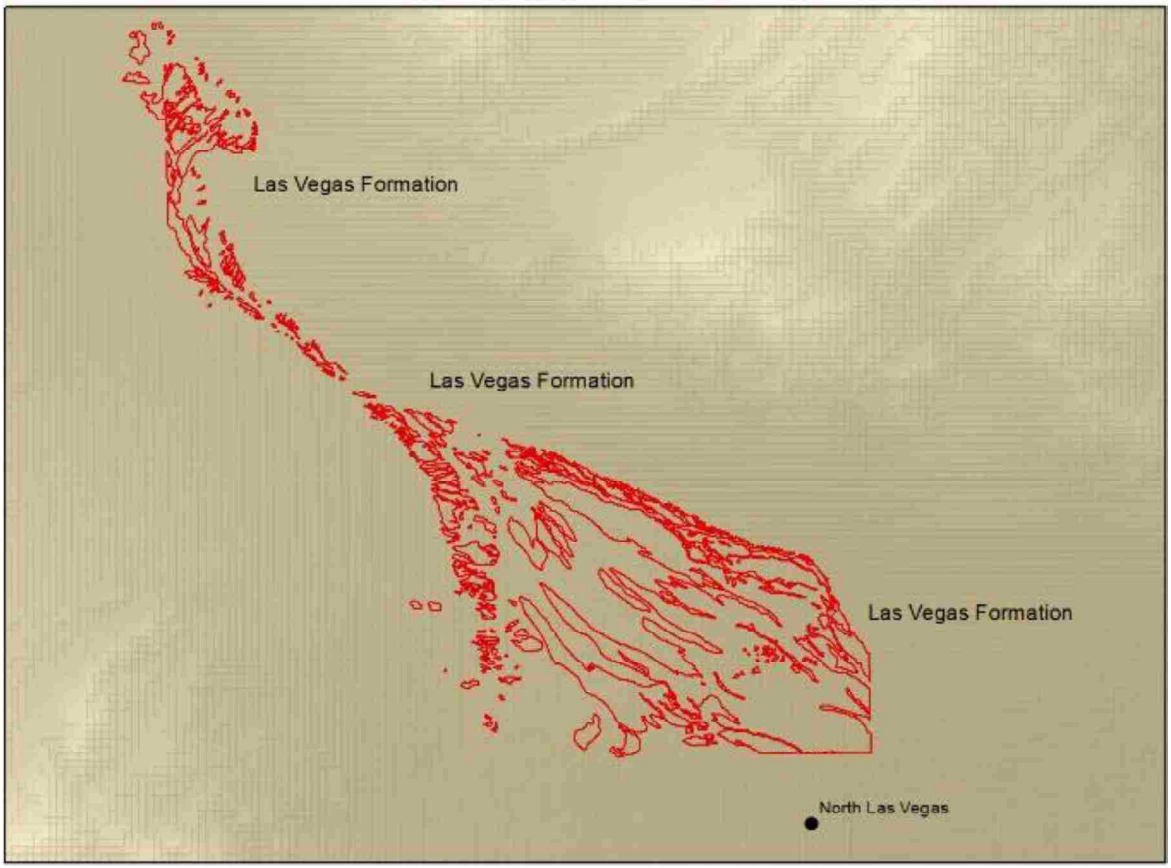

Figure 7: The Las Vegas Formation as derived from the 1:24k geologic map data

Methodology

(Pt. 2: Change Detection)

The goal of this land-use/land-cover impact analysis was to quantify the area within the LVfm that has experienced change due to urbanization. The boundary derived from digitizing the 1:24k geologic maps represents the most accurate definition of the LVfm based on available published geologic maps and the respective spatial coverage of those maps. I queried the EarthExplorer data portal for cloud-free, multi-temporal Landsat products. I conducted the subsequent image analysis using Environment of Visualizing Images (ENVI) software, now owned by Harris Geospatial. The ENVI image analysis software is widely used by GIS professionals and Remote Sensing Sciences.

The Landsat imagery showed that the area defined as the LVfm appears as a bright surface, in contrast to the surrounding basin fill and urban sprawl within Las Vegas Valley. I established a multi-temporal range with imagery in 5-year intervals, using years 1985, 1990, 1995, 2000, 2005, 2010. Landsat5 and for 2017. I also used 2017 imagery collected with the Landsat 8 OLI sensor. My objective was to obtain cloud-free imagery recorded in April, May and June. This window was chosen maximize signal response related to the acquisition timing of each pass of the Landsat sensor in relation to the solar zenith at that time of the year in the southwestern United States. The same range of April to June was chosen for the 2017 Landsat 8 OLI image. I radiometrically calibrated each image product from the level 1 digital number (DN) product into top of atmosphere radiance and then surface reflectance physical units.

Satellite sensors passively capture image data representing the Earth's surface, the calibrated DN's are not in physical units, thus these DN pixel values require calibration for further analysis. Radiometric calibration of the imagery significantly improves the researcher's ability to accurately quantify the observations made and to distinguish these observations from instrument-produced artifact or signal noise. (Borak et al., 2002). When sunlight reaches Earth's atmosphere, it interacts with atmospheric gasses. When the light arrives at the Earth's surface it interacts with physical surface features, and ultimately returns to the satellite's sensor after again interacting with Earth's atmospheric gasses. The light energy emitted by the sun radiates through space and is measured as a power density called irradiance (watts/meter^2), a measure of any light emitter of electromagnetic energy (EMR) (Richards, 2013). The actual physical unit of radiance accounts for the steradian variable (Richards, 2013). This assumes that incident irradiance is uniformly scattered, or equal amounts are distributed throughout equal cones at any incident angle. To calibrate the DN values to the physical unit of radiance, key assumptions are made. EMR on the path down to Earth's surface is scattered and the resulting pixel value will represent direct EMR and also EMR scattered throughout the path down to the surface. A pixel's value also integrates energy that has been reflected into it by surrounding objects. These EMR phenomena are accounted for as a mathematical variable in the DN to radiance conversion equation. Radiance values record changes to a pixel that has experienced any type of physical change to the surface that pixel represents (Mas et al., 1999).

Landsat DN pixel values (Q) for thematic mapper (TM) sensor is 8-bit ranges of 0-255. This range defines the Q_{cal}, Q_{calmin} and Q_{calmax}. Q_{calmin} is defined by the minimum

of the calibrated pixel value, and Q_{calmax} represents the maximum pixel value (Chander et al., 2009). The equation used to convert each selected Landsat scene from calibrated DN to spectral radiance is defined as

$$L_\lambda = \frac{LMAX\lambda - LMIN\lambda}{Qcalmax - Qcalmin}(Qcal - Qcalmin) + LMIN_\lambda$$

where L_λ is Spectral Radiance, Q_{cal} is the calibrated pixel value or Digital Number (DN), Q_{calmin} is the minimum DN pixel value in a given image, Q_{calmax} is the maximum DN pixel value in a given image, $LMIN_\lambda$ is the spectral at-sensor radiance scaled to Q_{calmin} , and $LMAX_\lambda$ is the spectral at-sensor radiance scaled to Q_{calmax}.

Conversion of the Landsat images from radiance to reflectance is simply a process of taking the ratio of measured radiance values by the solar irradiances above the atmosphere (Richards, 2013). This takes into account, the effects of atmospheric scattering and distortions caused by the absorptive behaviors of atmospheric gasses (Richards, 2013). The conversion to top of atmosphere (TOA) reflectance introduces advantages when working with multi-temporal image products. Chander et al., (2009) state that the three main advantages of converting radiance values to TOA reflectance are: 1) compensation for the cosine effect inherited by different solar zenith angles frequently observed in multi-temporal images. 2) Compensation for exoatmospheric solar irradiance and 3) Compensation for variation in Earth-Sun distances also observed in multi-temporal data sets. Conversion from radiance to TOA reflectance was executed using the equation defined as

$$P_\lambda = \frac{\pi \cdot L_\lambda \cdot d^2}{ESUN_\lambda \cdot \cos \theta_S}$$

where P_λ is TOA reflectance, π is the constant of pi, L_λ is the spectral radiance at sensor, d^2 is the Earth-Sun distance calculated by Julian year tables, $ESUN_\lambda$ is the mean exo-atmospheric solar irradiance, and $Cos\theta_s$ is the solar zenith angle in degrees.

Completion of radiometric calibration produced two new versions of each Landsat scene. In addition to the images representing Raw calibrated DN's, I now had images representing 1) radiance and 2) TOA reflectance. Howarth (1999) states that for a multi-temporal digital analysis, reflectance values should be used. As stated, the deposits within the area defined as the LVfm appear significantly brighter in contrast to surrounding physical elements in each Landsat scene. The 'brighter' appearance of the LVfm is a function of the surface illumination (*Fig. 8.)*

Figure 8: Google Earth Image of the LVfm and surrounding basin fill alluvium (to the north) and urban sprawl of Las Vegas and North Las Vegas (to the south).

Differences in surface illumination and other characteristics cause a change in radiance values (Singh et al., 1989). The illumination characteristic of the LVfm deposits was noted when attempting to determine which change detection methods are best suited for quantifying changes on such a surface. Due to the wide variety of change detection techniques that have been identified, it is important to identify which method best suits a specific environment (Zhang et al.,2009). These methods, the majority of which are based on the spectral information contained in each pixel, are built on the premise that any physical change in a ground feature will cause a measurable change in the corresponding pixel value (Zhang et al., 2009). Zhang et al. (2009) also point out that the study of urban/suburban land-use/land-cover changes are quite problematic due to the heterogeneous physical characteristics of land cover types within an urban/suburban area. The difficulties observed in change detection applications to heterogeneous surfaces are not significant in this study because the efforts here are not focused on quantifying specific changes in a heterogeneous urban/suburban surface, but simply a change in a 'bright', mostly homogeneous, sparsely vegetated surface of fine-grained groundwater discharge deposits.

The types of change detection techniques constructed for Landsat imagery are diverse; identification of the most appropriate methodology is a requirement for any monitoring program (Howarth et al., 1999). After reviewing the wide array of available change detection methods, I selected two methods that are the most effective for this project. The first component used in selecting which method was best suited is the physical characteristics of the surface of units defined as the LVfm. These surface

deposits are fine grained, groundwater-discharge deposits. They are sparsely vegetated and are observed to be bright, which results in significant contrast with urbanized land cover. Remote sensing research has indicated the effectiveness of vegetation indices in the characterization and measurement of the vegetation canopy (Huete et al., 1988). This ability to accurately identify and quantify vegetation canopy has been integrated into multiple change detection methods, such as vegetation index differencing (Singh et al., 1989). However, the LVfm units are sparsely vegetated, and the spatial resolution of the Landsat data sets spatial resolution is 30m/pixel. This spatial resolution would not be effective in accurately identifying vegetation through vegetation indices such as a normalized vegetation index. There are simply no areas of the LVfm that have a vegetation density near to, or greater, than 30 m. This observation negated the need to integrate vegetation index-based change detection into this project.

The second component was the spectral resolution of the Landsat imagery. Vegetation-Index-based change detection methods were not needed due to the lack of anextensive vegetation canopy, however the brightness of the surface is a physical characteristic that can yield quantifiable change through thresholding. If there are light objects in an image, light pixels on a dark background, then the objects may be extracted using simple thresholding (Singh 1989). Schowengerdt (1997) states that manual thresholding, allowing for the manual identification of the ideal threshold values, can also be effective as long as the threshold operator or image analyst has “a priori” knowledge of the scene. Image rationing, a ratio of two multi-temporal images, can effectively identify areas of change between dates by assigning a change value of greater than or less than 1 to areas, or pixels, that have experienced change between to

multi-temporal images (Singh 1989). The seven spectral wavebands for the selected Landsat sensors can yield additional image types derived from spectral transformations. The tasseled cap transformation has been widely used as a spectral compressing process that produces three bands based on the physical characteristics of the processed satellite scene (Ali-Baig et al., 2014). This transformation is effectively an orthogonal transformation by rotating each band into a new set of axes (Ali Baig et al., 2014). For Landsat 4 and 5 sensors, prior to calculating the tasseled cap transformation using the methods described by Huang et al. (2002), I calibrated both Landsat 4-5 DNs to the equivalent Landsat 7 DNs. This was required because different calibration methods were used for different Landsat missions. The conversion formula described by Vogelmann et al. (2001) calibrates Landsat 7 to Landsat 5 for purposes of quantification of radiometric and geometric artifacts in the Landsat 4-5 data sets. To calibrate from Landsat 5 to Landsat 7 DN equivalent values I used the inverse of Vogelmann's conversion formula. This process was described in detail by Firl and Carter (2011).

Table 2: Slope and intercept values described by Vogelmann et al. 2002. The inverse of these values were applied to convert Landsat 5 DN values to Landsat 7 DN values.

Landsat Band	Slope	Intercept	R^2
1	1.060	-4.21	0.9960
2	0.563	-2.58	0.9977
3	0.650	-2.50	0.9981
4	0.701	-4.80	0.9981
5	1.016	-6.96	0.9983
7	0.767	-5.76	0..9880

The inverse of the coefficients listed in *Table 3* were applied to the Landsat 5 data set using the formula $DN7 = (slope_\lambda * DN5) + intercept_\lambda$ described by Firl and Carter (2011). After Landsat 5 to Landsat 7 DN calibration was completed, I reapplied radiometric calibration methods to generate a Landsat 5 calibrated to Landsat 7 reflectance image. I then transformed the reflectance image into the brightness, wetness, and greenness band derived from the Huang et al. 2002 Tasseled Cap Transformation (TCT) process.

Table 3: Coefficients to construct Tasseled Cap brightness, greenness and wetness image data sets as described by Huang et al. 2002

TCT Band	Band 1	Band 2	Band3	Band4	Band5	Band7
Brightness	0.3561	0.3972	0.3904	0.6966	0.2286	0.1596
Greenness	-0.3344	-0.3544	-0.4556	0.6966	-0.0242	-0.2630
Wetness	0.2626	0.2141	0.0926	0.0656	-0.7629	-0.5388

I applied this transformation in order to extract the 'brightness' image for all of the multi-temporal data sets. The purpose in identifying the TCT as a viable method for image processing prior to change detection applications was to utilize the brightness contrast of the LVfm surface against the surrounding areas that have been impacted by urbanization. Including the TCT into the pre-change detection image processing provided three variations of image data sets: radiance, reflectance, and the TCT derived brightness. These three image-type variations are to be tested using the combination of image rationing and thresholding via manual density slicing to identify which produces the most accurate result.

I performed the image ratio calculations in ENVI. Prior to executing the ratio calculation using the band-math function, each image type required spectral subsetting followed by layer stacking. Spectral subsetting involves the selection of one single band from a multispectral image and generating a single image with that respective band. Layer stacking followed this spectral subset workflow by then stacking two multi-temporal images with corresponding image types, e.g., 1985_band_7_Radiance and 2010_band_7_Radiance. The layer stacking procedure was necessary for the band-math function to assign the selected bands to the ratio equation.

Once I identified the ideal change detection methods best suited for this study, my next step was to create a binary categorization of the LVfm surface to distinguish the land cover from the surface that is unchanged. I defined land within the boundary of the LVfm as “unchaged” if the land was observed to be in its natural, undisturbed state, or if the land is observed to have not been permanently altered by land-use/land-cover driven-processes. This would include land that has been altered or modified as a dirt road or a drainage easement, as these lands are not permanently covered or built over, thus leaving a potential for these lands to produce fossils. Any and all land that has been allocated for residential or commercial infrastructure, built upon, or paved over is considered “changed” surface in this study. I utilized hi-resolution National Agriculture Imagery Program (NAIP) aerial imagery and Google Earth to verify my binary classification methods of the LVfm surface. An example of LVfm surface I identified as “unchanged” can be seen within the transparent red boundary from Google Earth (*Fig. 9.)* An image representing surface considered “changed” which includes land graded for residential conversion that is yet to be permanently altered, is provided in Figure 10.

Figure 9: Image of LVfm established as unchanged (red transparent area within boundary adjacent to residential neighborhood.

Figure 10: Land categorized as changed via permanent alteration by land-use/land-cover (area within transparent red polygon).

I processed all the allocated LiDAR data using the binary land classification of ‘changed’ and ‘unchanged’. This resulted in a polygon boundary for measurement of land-cover/land-use change in terms of lands affected and unaffected. The extent of the LiDAR coverage terminates near the northwest border of the Paiute Tribal Golf course about 25 km northwest of Las Vegas. The outcrops of LVfm that occur northwest of this area have experienced no observed changes in terms of land-use/land-cover as observed through recent high-resolution aerial NAIP imagery. The southern extent boundary of the LiDAR provides consistent coverage for all remaining LVfm outcrops. It is these outcrops of LVfm following the Las Vegas Wash trending (southeast) that have been observed to have experienced the most significant impacts from land-use/land-cover change. The first steps in processing the LiDAR was to quality check the point classification for errors. The LiDAR data sets, downloaded through the Earthexplorer data portal, were analyzed in ESRI ArcMap using the ArcScan and 3D analyst tools. Additionally, I acquired an open source set from https://rapidlasso.com/lastools/ of tools created for ingestion into ArcMap as an ArcToolbox.

Each footprint of all individual LiDAR files was post-processed prior to downloading from Earthexplorer, meaning each point was classified as ground, building, high, medium or low vegetation, etc. (*Fig. 11*). Because the goal of this project is to assess any change to LVfm outcrops, the differentiated point classes are not needed. I implemented a point classification re-assignment by intersecting NAIP imagery acquired in July 2010 with the LiDAR point cloud. Application of the multi-sensor data fusion described by Yan et al. (2015) integrated the SNWA LiDAR product with the NAIP

imagery for manual classification. The NAIP imagery provided 1m resolution; the LiDAR data product is sub-meter in x, y, and z accuracies. This inverse spatial relationship does not violate the spatial resolution criteria mentioned by Yan et al. (2015). I drew cross-sections over areas identified as representing urbanization, land-use/land-cover changes. I assigned the LiDAR points over each area a binary point classification. Assigning all LiDAR points a category of changed or unchanged. This point classification method ensured that all points observed to represent land-use/land-cover change were accurately identified as they were intersected with NAIP imagery (*Fig. 12*).

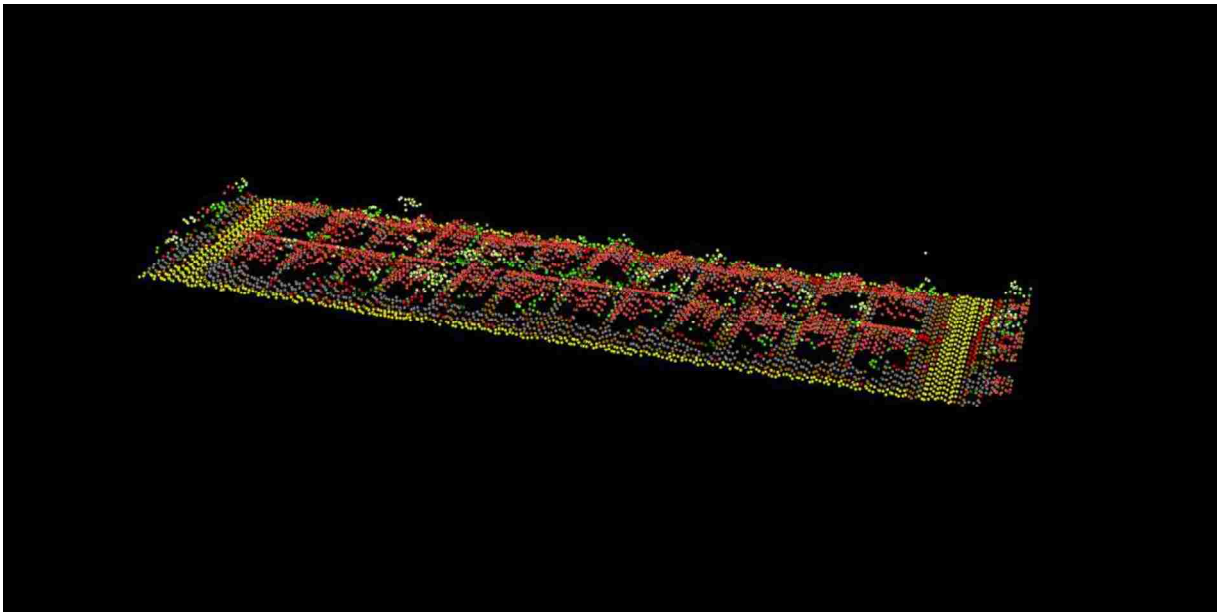

Figure 11: 3-Dimensional view of point classifications observed in the SNWA LiDAR product.

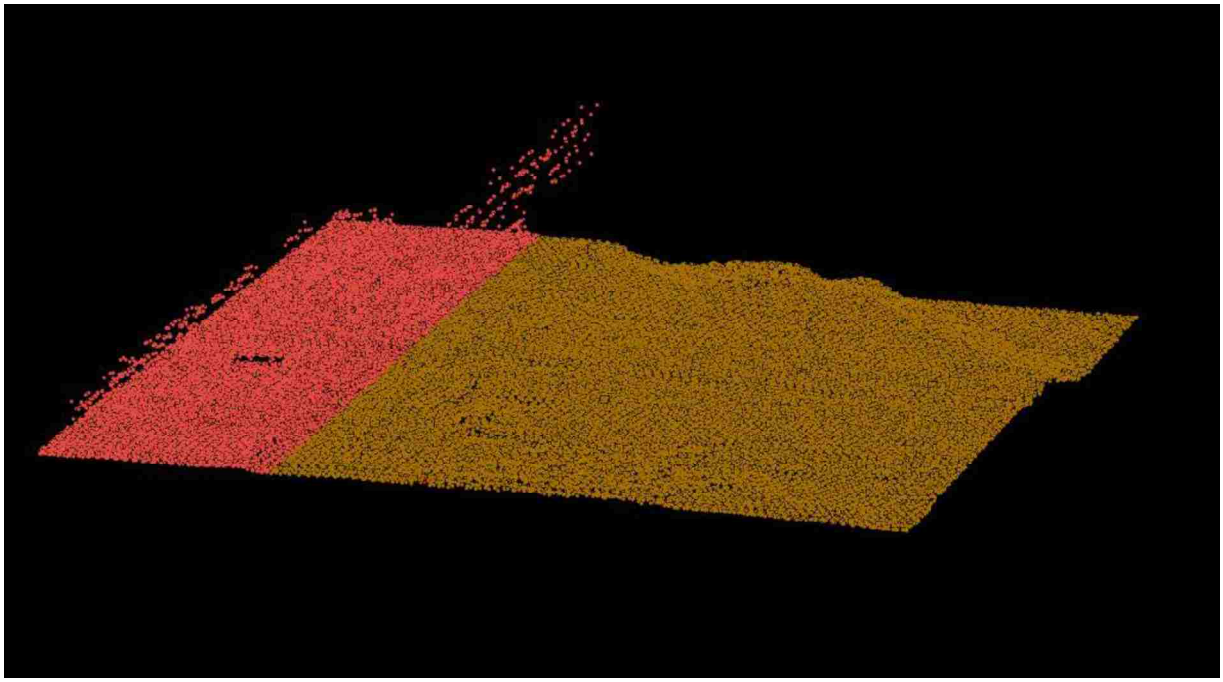

Figure 12: Bulk binary classified 3-D point cloud. Ground classification (right) and points classified to represent change (left). Note: High points are high voltage transmission power lines adjacent to residential subdivision.

I entered the bulk binary classified LiDAR points into a conversion tool that extracted the classed points out of the LiDAR data set and produced a multipoint feature class in ArcGIS. A multipoint feature class is associated with mass point observations such as LiDAR point clouds, and contains multipoint geometry, in this case horizontal x, y, and vertical z. The final step was to convert the multipoint feature class into a polygon shapefile. For this conversion I utilized the aggregate point tool in ESRI's ArcGIS. The input aggregation distance was set at 30 m in order to generate a polygon that was sampled compatibly with the 30 m spatial resolution of the Landsat images. This procedure generated what is considered a ground-truth boundary, defining human-generated land-use/land-cover that can be measured against the boundary of the LVfm.

Beginning with the 2010 Landsat image, the image date that corresponds to the acquisition year of the LiDAR acquisition, I conducted a change detection analysis using Image rationing and manual thresholding. I measured this first result against the LiDAR-derived boundary as an accuracy assessment.

The first iteration, using image ratio change detection, focused on the Landsat 5 image from May 18, 1985 against the Landsat 5 May 7, 2010 image. The application of the change detection methods were then applied to the reflectance, radiance, and the TCT-derived brightness bands. For the radiance and reflectance images, I calculated the image ratio using bands 5 and 7 shortwave infrared 1.55 µm-1.75 µm and 2.08 µm - 2.35 µm, respectively, in SWIR. The bright surface of the LVfm as it appears in the Landsat images suggests using the SWIR bandwidths, not only because the deposits appear bright in contrast, but also because they represent dry ephemeral washes. The SWIR wavelength region has been highly correlated with the moisture content of soil surfaces (Khanna et al., 2007). I linked the rationing result image to a display of the 2010 image in ENVI for manual threshold analysis. I then overlaid the rationing result image using the density slice overlay option, which designates all pixel value ranges within an image into a default 8 range (*Fig. 13*).

I reviewed each assigned range value were with the linked display to ensure that the pixels were assigned a correct value in terms of ‘changed’ or ‘unchanged’. Pixels that correctly classified and represented unchanged areas were grouped and assigned to a black color value; pixels representing changed areas were assigned a red color value. During this process, for each image I further differentiated multiple density slice ranges into four or more sliced ranges to re-assign the correct value of change for a particular pixel(s) (*Fig. 14*). This corrected for pixels that were incorrectly classified as not changed. It also enabled me to re-classify pixels into the appropriate range of changed pixels. I applied this process to each image type, and I exported the result of each process as a shapefile from ENVI for ingestion into ArcGIS. This allowed me to quantify the area of the change-detection result and compare it to the LiDAR-derived ground-truth boundary.

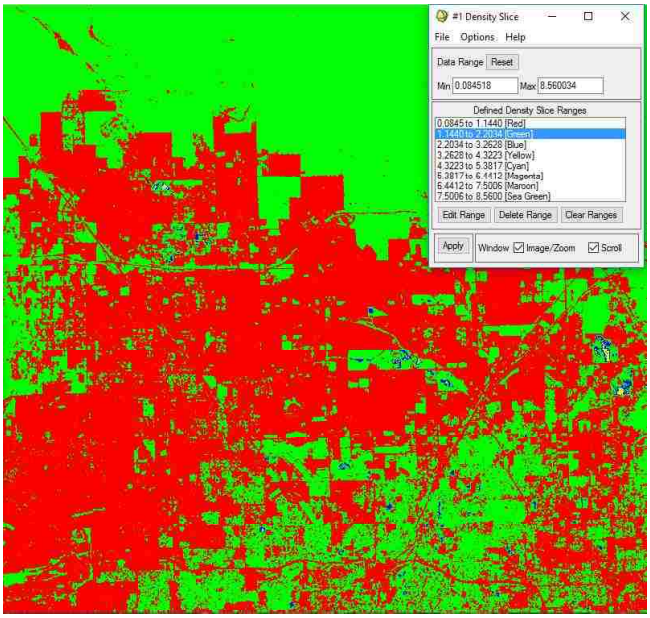

Figure 13: Default density slice overlay in ENVI of Ratio result from Band 5 SWIR 1985/Band 5 SWIR 2010.

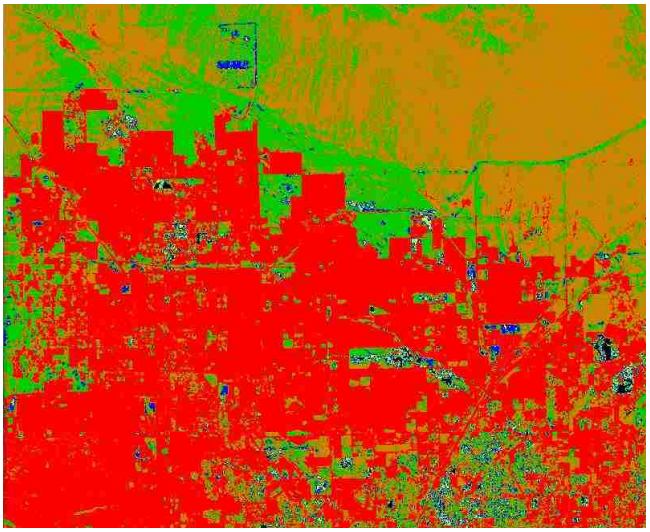

Figure 14: Differentiation of Density Slice Ranges. In Figure 14 the green density slice range of 1.1140-2.2034 was differentiated into 5 individual ranges to further aid in accurate threshold classification.

Results

The land-use/land-cover boundary derived from processing the 2010 LiDAR data set processing was calculated to have a total area of 34.388 km^2. This calculation was measured against the total area of the 1:24k-scale boundary defining the LVfm. This resulted in a quantified percentage of area impacted by land-use/land-cover change of 52.19%, as of 2010. Change-detection methodology was applied to the first multi-temporal Landsat image which measured the 1985 image against the 2010 image. The image ratio and manual thresholding technique was applied to the band 5 and 7 reflectance, radiance, and the TCT-derived 'brightness' images results listed in *Table 4*.

Table 4: Image ratio/thresholding results for first iteration of change detection.

Image Date	Band	Image Type	Area M^2	Area Km^2
1985 v 2010	5	Radiance	32059138.13	32.0591
1985 v 2010	5	Reflectance	34095158.89	34.0951
1985 v 2010	brightness	Tasseled Cap	34205299.96	34.2052
1985 v 2010	7	Radiance	32770677.87	34.3222
1985 v 2010	7	Reflectance	39656373.5	33.8028

The calculated area derived from change detections performed on SWIR radiance, reflectance, and TCT 'brightness' were calculated against the area calculated from the LiDAR ground truth area. All area calculations were made in ArcGIS with all

data being projected to NAD83 UTM Zone 11 N. Review of the initial change-detection results indicated that the most accurate results were derived from the TCT 'brightness' band, band 5 reflectance, and band 7 radiance ratios. Band 5 radiance and band 7 reflectance images produced less accurate results, a difference of ± 3 km^2. For each image type, a percentage difference was also calculated to produce a quantified justification for using only the TCT 'brightness', band 5 reflectance, and band 7 radiance images for all change-detection iterations. The percent differences are calculated in *Table 5*. This table illustrates that band 7 radiance produced the most accurate result, compared to the LiDAR ground truth boundary, with only a 4.9% difference in area between the two data sets.

Table 5: Resulting calculations of the total percentage of change within the LVfm boundary compared to LiDAR ground truth percentage of impacted area. The percent difference indicates that the TCT 'brightness' band and the B5 Reflectance and B7 Radiance

Image Date	Band	Image Type	% Impacted Area	% Difference
1985 v 2010	5	Radiance	48.6558Km^2	11.2055
1985 v 2010	5	Reflectance	51.7458Km^2	5.5663
1985 v 2010	Brightness	Tasseled Cap	51.913Km^2	5.2612
1985 v 2010	7	Radiance	52.0905	4.9373
1985 v 2010	7	Reflectance	51.3023Km^2	6.7358
2010	N/A	LiDAR	54.7960Km^2	0

The TCT ‘brightness, band 7 radiance, and band 5 reflectance produced an average percent difference of 5.25% from the LiDAR ground-truth data set. The aforementioned change detection methods were then applied to the remaining Landsat scenes for 1990, 1995, 2000, 2005, and 2017, using the TCT–brightness, and the B5 reflectance areas were calculated for all years. The calculated areas of change (*Fig.15*) show a rapid increase in land-use/land-cover change between years 2000 and 2005.

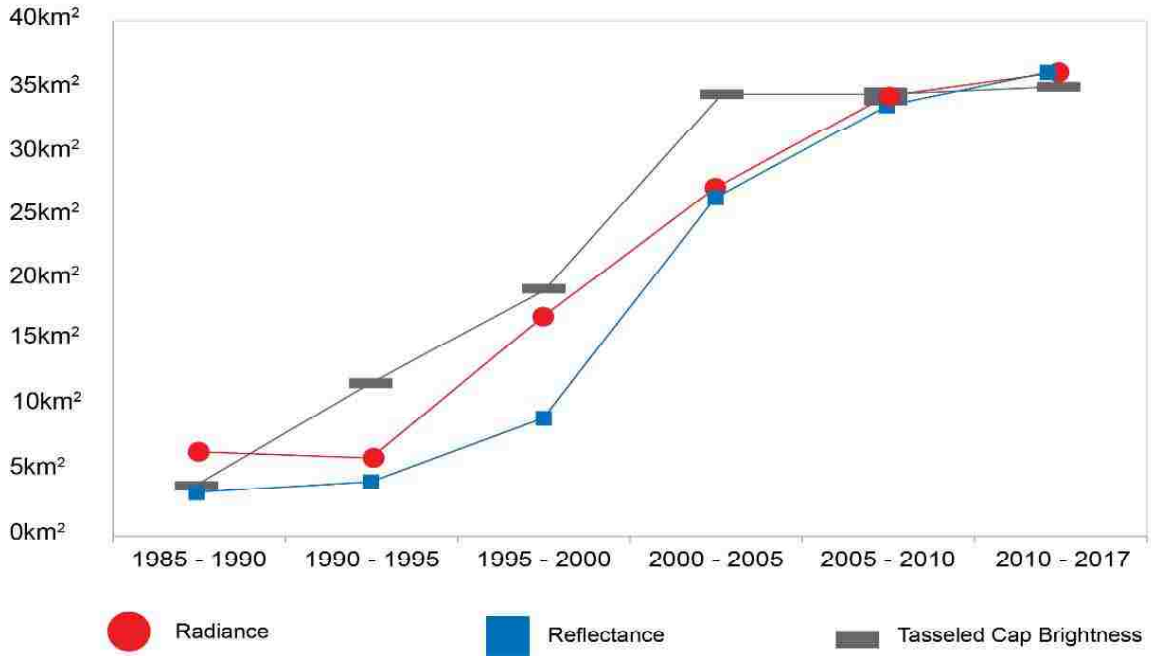

Figure 15: Radiance, Reflectance, Brightness Change detection results

All three image types recorded a positive linear trend, with the most significant increases occurring between 1990 and 2010. The first change-detection iteration measured change from 1985 to 1990 and recorded 4.44 km^2 (the average of all three image types used in my analysis). From 1985 to 1995 the averages of all three image types recorded 7.32 km^2 of area within the LVfm that had experience land-use/land-cover impact. The average change in area was calculated for the remainder of all multi-temporal change detection results. These averages were then compared to identify in which five year time interval the rate of impact was highest. The comparison was calculated by taking the average from each multi-temporal change-detection result (*Fig. 15*). The difference in impacted area from 1985 to 1990 was 2.87km^2. From 1990 to 1995 the area of impact was calculated to be 4.33 km^2. From 1995 to 2000 the area of land-cover/land-use impact jumped to 3.57 km^2 for that five year interval. The next two five year intervals, 2000 to 2005 and 2005 to 2010, the area affected by land-use/land-cover change signficantly dropped to ~ 1 km^2 and less than 0.5 km^2, respectively

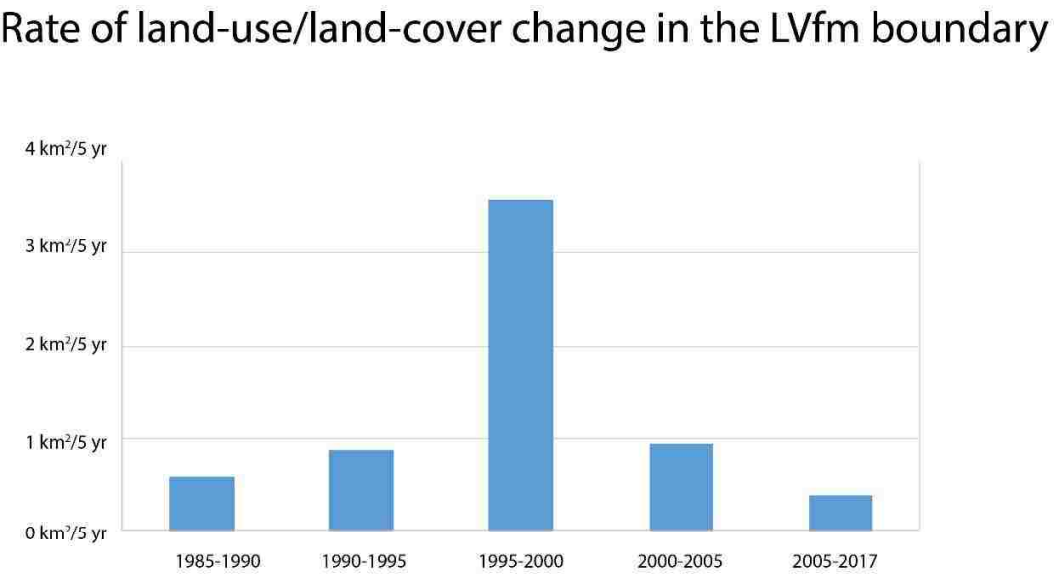

Figure 16: Rates of land-use/land-cover impact in the LVfm for 5- year intervals beginning in 1985

Discussion

The change-detection component to this project demonstrated the versatility of the PFYC project. This project extracted a spatial relationship between the LVfm and the City of Las Vegas. This spatial proximity provided an opportunity to investigate effects of rapid urbanization within the LVfm boundary. This project utilized the spectral, spatial and multi-temporal capabilities of remotely sensed images to measure land-use/land-cover changes over time. Additionally, this project implemented a multi-sensor urban classification methodology that integrated aerial LiDAR and high-resolution imagery to generate a ground-truth boundary from which accuracy assessments could be generated. The initial change-detection results identified two SWIR bandwidths, one reflectance, one radiance, as well a 'brightness' image, to produce the most accurate measurement of land-use/land-cover change within the LVfm. These results, compared to the LiDAR ground truth, indicate that this combination of change detection techniques can produce accurate measurements of land-use/land-cover changes. This project acknowledges the inherent difficulties experienced by researchers in quantifying land-use/land-cover changes within heterogeneous urban surfaces. In contrast, in this project I simply measured any physical change related to urbanization in a bright, sparsely vegetated surface that represents Pleistocene groundwater-discharge deposits of the Las Vegas Formation.

Mutli-temporal analysis produced a measured change in the area impacted by land-use/land-cover brought on by rapid urbanization that closely parallels population growth rates. All change-detection results indicate positive trends from 1985 to 2017. As shown in Figure 16, the percentage of area impacted by land-use/land-cover shows

distinct, significant increases over specific time intervals. These observations correspond to large population increases that occurred within the temporal range of this study. The most significant growth rates have been reported as 61.1%, 85.5% and 41.8% during the 1980-1990, 1990-2000 and 2000-2010 intervals, respectively (Frey, 2012). Las Vegas recorded the 4th, and 1st highest growth rates for the decades 1980 to 1990 and 1990 to 2000 (*Fig. 17*).

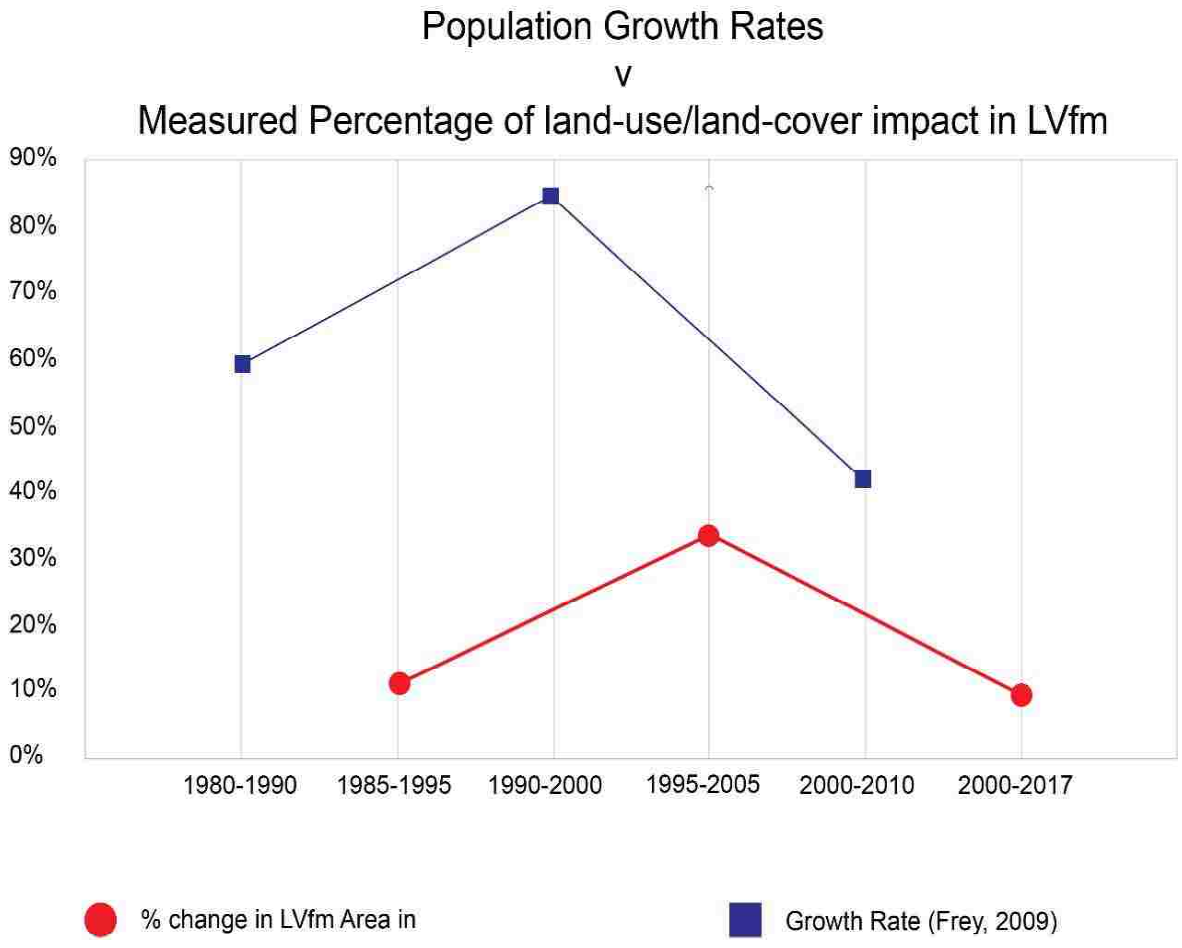

Figure 17: Growth Rates for Las Vegas (Frey, 2009) plotted against calculated percentage or area impacted inside boundary of LVfm

The plot in *Figure 17* describes the rates of land-use/land-cover impacts as a result of population growth. The temporal relationship between the percentage change in the Las Vegas Formation area and growth rates is a function of turnover time. The time between population growth and the subsequent development that takes place to accommodate the new population.

The economic downfall that began in 2008 spawned from mortgage-related securities, significantly impacted the U.S. and global financial markets (Kotz, 2009). The resulting 'Great Recession' significantly impacted growth in Las Vegas and slowed the rate of urbanization in terms of land-use/land-cover change. This slow-down is distinctly apparent in the TCT brightness plot (*Fig.16*). Additionally, the calculated area of land-use/land-cover change is consistent with the population numbers recorded by Frey (2012). From 2001-2004 Las Vegas reported the fastest population growth in the Mountain West and one of the highest population growth rates nationally (Frey, 2012).

The correlation between the amounts of land-use/land-cover impact calculated from the CD methods utilized in this project and the population growth observed in Las Vegas was expected. The relationship between population growth and rapid urbanization is well documented. Shown by these results, after a time of rapid population growth, the local area will respond with a time of rapid land-use/land-cover urbanization. These data generated in this study demonstrate the value of multi-temporal, remotely-sensed, image analysis and its effectiveness in documenting and quantifying changes in urbanizing landscapes.

Appendix A: Bureau of Land Management Standard Scope of Work (PFYC) Project

vPFYC Feature Class Polygons					
NEW GIS Name	**Alias**	**Data Format**	**Required ?**	**Domain Values**	**Comments**
PFYC_CLASS_CD	PFYC	Char(1)	Yes	1 2 3 4 5 I W U	Autopopulates from the selection made in the PFYC_JUST_TX choice. The assigned value for the Potential Fossil Yield Classification for the rock unit. Standard colors for the symbology are: 1 Yucca Yellow; 2 Mango; 3 Electron Gold; 4 Flame Red; 5 Tuscan Red; I Snowfield/ice; W lake; U Gray 40%. No outlines on the PFYC classes, but

					outline water and ice polygons
PFYC_JUST_TX	PFYC Justification	Char(50)	Yes	Appendix 3	Provides a simple explanation for the assigned PFYC value. Multiple values might reasonably apply but pick the one value that is most applicable.
PALEO_COMMENT_TX	Comments	Char(1000)	No		Area to provide short comments related to the paleontology resource. E.g., “Dinosaurs common,” “Significant plants known,” or “Common invertebrates occur regularly,” etc.

GEO_UNIT_NM	Geologic Unit Name	Char(100)	Yes		Either the Formation name or the name/description of the rock unit mapped (e.g., Quaternary alluvium)
GEO_DESC_TX	Description	Char(2000)	Yes		Description of the rock unit, generally derived from the explanation of the source map. May include significant faces information and/or geographic variations
EARLIEST_AGE_NM	Earliest Age	Char(100)	Yes	Appendix 1	Name of the Geologic time period (e.g., Cretaceous, or Zanclean, etc.) that corresponds to the

					earliest geologic age of the unit mapped.
EARLIEST_AGE_NR	Earliest Age Sort Code	Double(9)	Yes	Appendix 1	Numeric code given to the specific time period selected for the EarliestAge, populated automatically based upon choice there
LATEST_AGE_NM	Latest Age	Char(100)	Yes	Appendix 1	Name of the Geologic time period (e.g., Cretaceous, or Zanclean, etc.) that corresponds to the latest geologic age of the unit mapped. This would be different than the EarliestAge when the mapped rock

					unit is known to cross time periods
LATEST_AGE_NR	Latest Age Sort Code	Double(9)	Yes	Appendix 1	Numeric code given to the specific time period selected for the LatestAge, populated automatically based upon choice there
GEN_COMMENT_TX	Comment	Char(1000)	NO		General comments: May include comments related to rational of PFYC ranking; information related mapping of combination of units; management considerations beyond those covered by PFYC classifications, etc.

ORIG_GEO_SYMB_CD	Original Geology Symbol	Char(10)	Yes		Comes from the original source map
MAP_REF_CD	Map Reference Code	Char(15)	Yes		This code is created by combining the 2 letter state code, the first 4 characters of the primary map author's last name, plus the first and middle initial, plus the 4 digit year of publication. Example: MTHamiJA1960. If there are multiple source maps by the same author in the same year, append a letter after the year to differentiate between them.

					Example MTHamiJA1960a.
GEO_CD	Geologic Code	Char(25)	Yes		It is created by combining the 2-letter abbreviation for the state, the Map Reference Code (above) and the original geologic symbol from the source map. Example: MTHamiJA1960Kgr. This will automatically distinguish this map's concept of Kgr from any other in the data set, giving a unique code for these units across the entire data set. By convention, the first

					letter of the geologic code from the source map will represent the rock unit's geologic age. Occasionally the characters are not easily convertible alphanumeric characters. If that is the case, see Appendix 2 for recommended characters for the Geologic age portion of the code
STATE_CD	State	Char(2)	Yes		State
RuleID_CD	Rule ID	Char(1)	No		This is an ESRI field that allows for

Map Index Feature Class Polygons

NEW GIS Name	Alias	Data Format	Required ?	Domain Values	Comments
MAP_REF_CD	Map Reference Code	Char(11)	Yes		This code is identical to the code created in the PFYC Feature Class, by combining the 2 letter state code, the first 4 characters of the primary map author's last name, plus the first and middle initial, plus the 4 digit year of publication. Example: MTHamiJA1960. If there are multiple source maps by the same

					author in the same year, append a letter after the year to differentiate between them. Example MTHamiJA1960a .
FIRST_AUTH_NM	First Author	Char(35)	Yes		Contains the last name, followed by the first and middle initials of the primary author of the source map. Example: Hamilton, JA
OTHER_AUTH_NM	Other Authors	Char(100)	No		Enter all other authors in this field as last name, initials. Separate authors by

					semicolon. Example: Hammond, PE; Ferns, ML
PUB_DT	Publication Date	Date	No		Date of publication for the source map. If exact publication date is not known, enter 01/01/year where the year is the numeric year of publication. If the source map is unpublished leave value null
TITLE_TX	Title	Char(200)	Yes		Title of the source map. If unknown enter unknown.
PUB_NM	Publisher	Char(100)	No		The organization responsible for producing the map. Example:

					U.S. Geological Survey
SERIES_TX	Series	Char(100)	No		Name of the series or journal. Example: Professional Paper
SERIES_NR	Series Number	Char(20)	No		Number of the series or volume of the journal
PUB_LOC_TX	Place	Char(100)	No		Place of publication
MAP_SCALE_NR	Source Scale	LongInteger(7)	Yes		The scale of the source map. If the map is 1:24,000 then enter "24000" as the scale
DIGITIZER_NM	Digitizer Name	Char(100)	No		Name or source of the person or entity that digitized the

					published map if known
DIGITIZER_DT	Digitized Date	Date	No		Date that the digital data was finalized if known. If only year is known enter 1/1/year
MAP_URL_OBJECT	Map URL	Char(250)	No		If it is available put in the public web address of the source map. Example: address from the USGS National Geologic Map Database
LABEL_NM	Label	Char(100)	Yes		This field would be used to label the layer in ArcMap. The label would be the name of the map followed by

					the scale, like "Alzada 100k"

Standard numerical codes were created for all of the divisions of geologic time from Age to Eon. When sorted numerically from smallest to largest the result is a proper ordering of the time units. If these time names and sort codes are associated with rock units in a geologic map, then the units can be sorted in close stratigraphic order. The sort code consists of 8 or more digits. The digit in the highest position relates to the Eras of the Phanerozoic or the Eons of the Precambrian. So, numbers beginning with 1 relate to the Cenozoic, 2 the Mesozoic, up to 11 for the Hadean. The next 2 digits relates to the Period. For the Cenozoic, 10 would be the Quaternary, 20 is the Neogene, and 30 is the Paleogene. Beginning in the Mesozoic the numbers start again with 10 for the Cretaceous and so on. The next 3 digits relate to the Epoch. In the Cenozoic, 100 is the first Epoch, or the Pliocene, and 200 begins the Miocene sequence. In the Mesozoic, 100 marks the Late Cretaceous, and so on. The final 2 digits relate to the Age, so for the Pleistocene the 2 ages are represented by 20 and 30 respectively. The reason for having large gaps in the numbers, like between 100 for Pliocene and 200 for Miocene, is to provide flexibility in the event that other units need to be inserted in the future.

When selecting which time name to apply to a mapped geology unit there is several considerations. In general, apply the most precise name you can. If a map author only maps a unit as Cretaceous do not be any more precise without other evidence, and mark the unit as Cretaceous in both the EarliestAge and the LatestAge fields. If based upon your knowledge of a unit you can confidently give it a more precise name, do so while making a note as to your choice. Also, sometimes geology units cross time boundaries, or were mapped as a lumped unit. In those cases, put the appropriate values in the EarliestAge and LatestAge fields.

Time Name	Sort
Cenozoic	10000000
Quaternary; Cenozoic	11000000
Holocene; Quaternary; Cenozoic	11010000
Pleistocene; Quaternary; Cenozoic	11020000
Rancholabrean LMA	11020001
Irvingtonian LMA	11020002
Blancan LMA	11020003
Calabrian; Pleistocene; Quaternary; Cenozoic	11020020
Gelasian; Pleistocene; Quaternary; Cenozoic	11020030
Neogene; Cenozoic	12000000
Pliocene; Neogene; Cenozoic	12010000
Hemphillian LMA	12010001
Piacenzian; Pliocene; Neogene; Cenozoic	12010010
Zanclean; Pliocene; Neogene; Cenozoic	12010020
Miocene; Neogene; Cenozoic	12020000
Messinian; Miocene; Neogene; Cenozoic	12020010
Tortonian; Miocene; Neogene; Cenozoic	12020020
Clarendonian LMA	12020021
Serravallian; Miocene; Neogene; Cenozoic	12020030
Barstovian LMA	12020031
Langhian; Miocene; Neogene; Cenozoic	12020040
Burdigalian; Miocene; Neogene; Cenozoic	12020050
Hemingfordian LMA	12020051

Aquitanian; Miocene; Neogene; Cenozoic	12020060
Paleogene; Cenozoic	13000000
Oligocene; Paleogene; Cenozoic	13010000
Chattian; Oligocene; Paleogene; Cenozoic	13010010
Arikareean LMA	13010011
Geringian LMA	13010012
Orellan LMA	13010013
Rupelian; Oligocene; Paleogene; Cenozoic	13010020
Eocene; Paleogene; Cenozoic	13020000
Priabonian; Eocene; Paleogene; Cenozoic	13020010
Chadronian LMA	13020011
Bartonian; Eocene; Paleogene; Cenozoic	13020020
Duchesnean LMA	13020021
Uintan LMA	13020022
Lutetian; Eocene; Paleogene; Cenozoic	13020030
Bridgerian LMA	13020031
Ypresian; Eocene; Paleogene; Cenozoic	13020040
Paleocene; Paleogene; Cenozoic	13030000
Wasatchian LMA	13030001
Thanetian; Paleocene; Paleogene; Cenozoic	13030010
Clarkforkian LMA	13030011
Tiffanian LMA	13030012
Selandian; Paleocene; Paleogene; Cenozoic	13030020
Torrejonian LMA	13030021

Puercan LMA	13030022
Danian; Paleocene; Paleogene; Cenozoic	13030030
Mesozoic	20000000
Cretaceous; Mesozoic	21000000
Upper Cretaceous; Cretaceous; Mesozoic	21010000
Maastrichtian; Upper Cretaceous; Cretaceous; Mesozoic	21010010
Lancian LMA	21010011
Campanian; Upper Cretaceous; Cretaceous; Mesozoic	21010020
Santonian; Upper Cretaceous; Cretaceous; Mesozoic	21010030
Judithian LMA	21010031
Aquilian LMA	21010032
Coniacian; Upper Cretaceous; Cretaceous; Mesozoic	21010040
Turonian; Upper Cretaceous; Cretaceous; Mesozoic	21010050
Cenomanian; Upper Cretaceous; Cretaceous; Mesozoic	21010060
Lower Cretaceous; Cretaceous; Mesozoic	21020000
Albian; Lower Cretaceous; Cretaceous; Mesozoic	21020010
Aptian; Lower Cretaceous; Cretaceous; Mesozoic	21020020
Barremian; Lower Cretaceous; Cretaceous; Mesozoic	21020030
Hauterivian; Lower Cretaceous; Cretaceous; Mesozoic	21020040
Valanginian; Lower Cretaceous; Cretaceous; Mesozoic	21020050
Berriasian; Lower Cretaceous; Cretaceous; Mesozoic	21020060
Jurassic; Mesozoic	22000000
Upper Jurassic; Jurassic; Mesozoic	22010000
Tithonian; Upper Jurassic; Jurassic; Mesozoic	22010010

Kimmeridgian; Upper Jurassic; Jurassic; Mesozoic	22010020
Oxfordian; Upper Jurassic; Jurassic; Mesozoic	22010030
Middle Jurassic; Jurassic; Mesozoic	22020000
Callovian; Middle Jurassic; Jurassic; Mesozoic	22020010
Bathonian; Middle Jurassic; Jurassic; Mesozoic	22020020
Bajocian; Oxfordian; Upper Jurassic; Jurassic; Mesozoic	22020030
Aalenian; Middle Jurassic; Jurassic; Mesozoic	22020040
Lower Jurassic; Jurassic; Mesozoic	22030000
Toarcian; Lower Jurassic; Jurassic; Mesozoic	22030010
Pliensbachian; Lower Jurassic; Jurassic; Mesozoic	22030020
Sinemurian; Lower Jurassic; Jurassic; Mesozoic	22030030
Hettangian; Lower Jurassic; Jurassic; Mesozoic	22030040
Triassic; Mesozoic	23000000
Upper Triassic; Triassic; Mesozoic	23010000
Rhaetian; Upper Triassic; Triassic; Mesozoic	23010010
Norian; Upper Triassic; Triassic; Mesozoic	23010020
Carnian; Upper Triassic; Triassic; Mesozoic	23010030
Middle Triassic; Triassic; Mesozoic	23020000
Ladinian; Middle Triassic; Triassic; Mesozoic	23020010
Anisian; Middle Triassic; Triassic; Mesozoic	23020020
Lower Triassic; Triassic; Mesozoic	23030000
Olenekian; Lower Triassic; Triassic; Mesozoic	23030010
Induan; Lower Triassic; Triassic; Mesozoic	23030020
Paleozoic	30000000

Permian; Paleozoic	31000000
Lopingian; Permian; Paleozoic	31010000
Changhsingian; Lopingian; Permian; Paleozoic	31010010
Wuchiapingian; Lopingian; Permian; Paleozoic	31010020
Guadalupian; Permian; Paleozoic	31020000
Capitanian; Guadalupian; Permian; Paleozoic	31020010
Wordian; Guadalupian; Permian; Paleozoic	31020020
Roadian; Guadalupian; Permian; Paleozoic	31020030
Cisuralian; Permian; Paleozoic	31030000
Kungurian; Cisuralian; Permian; Paleozoic	31030010
Artinskian; Cisuralian; Permian; Paleozoic	31030020
Sakmarian; Cisuralian; Permian; Paleozoic	31030030
Asselian; Cisuralian; Permian; Paleozoic	31030040
Carboniferous; Paleozoic	31500000
Pennsylvanian; Carboniferous; Paleozoic	32000000
Upper Pennsylvanian; Pennsylvanian; Carboniferous; Paleozoic	32010000
Gzhelian; Upper Pennsylvanian; Pennsylvanian; Carboniferous; Paleozoic	32010010
Kasimovian; Upper Pennsylvanian; Pennsylvanian; Carboniferous; Paleozoic	32010020
Middle Pennsylvanian; Pennsylvanian; Carboniferous; Paleozoic	32020000
Moscovian; Middle Pennsylvanian; Pennsylvanian; Carboniferous; Paleozoic	32020010
Lower Pennsylvanian; Pennsylvanian; Carboniferous; Paleozoic	32030000
Bashkirian; Lower Pennsylvanian; Pennsylvanian; Carboniferous; Paleozoic	32030010
Mississippian; Carboniferous; Paleozoic	33000000
Upper Mississippian; Mississippian; Carboniferous; Paleozoic	33010000

Serpukhovian; Upper Mississippian; Mississippian; Carboniferous; Paleozoic	33010010
Middle Mississippian; Mississippian; Carboniferous; Paleozoic	33020000
Visean; Middle Mississippian; Mississippian; Carboniferous; Paleozoic	33020010
Lower Mississippian; Mississippian; Carboniferous; Paleozoic	33030000
Tournaisian; Lower Mississippian; Mississippian; Carboniferous; Paleozoic	33030010
Devonian; Paleozoic	34000000
Upper Devonian; Devonian; Paleozoic	34010000
Famennian; Upper Devonian; Devonian; Paleozoic	34010010
Frasnian; Upper Devonian; Devonian; Paleozoic	34010020
Middle Devonian; Devonian; Paleozoic	34020000
Givetian; Middle Devonian; Devonian; Paleozoic	34020010
Eifelian; Middle Devonian; Devonian; Paleozoic	34020020
Lower Devonian; Devonian; Paleozoic	34030000
Emsian; Lower Devonian; Devonian; Paleozoic	34030010
Pragian; Lower Devonian; Devonian; Paleozoic	34030020
Lochkovian; Lower Devonian; Devonian; Paleozoic	34030030
Silurian; Paleozoic	35000000
Pridoli; Silurian; Paleozoic	35010000
Ludlow; Silurian; Paleozoic	35020000
Ludfordian; Ludlow; Silurian; Paleozoic	35020010
Gorstian; Ludlow; Silurian; Paleozoic	35020020
Wenlock; Silurian; Paleozoic	35030000
Homerian; Wenlock; Silurian; Paleozoic	35030010
Sheinwoodian; Wenlock; Silurian; Paleozoic	35030020

Llandovery; Silurian; Paleozoic	35040000
Telychian; Llandovery; Silurian; Paleozoic	35040010
Aeronian; Llandovery; Silurian; Paleozoic	35040020
Rhuddanian; Llandovery; Silurian; Paleozoic	35040030
Ordovician; Paleozoic	36000000
Upper Ordovician; Ordovician; Paleozoic	36010000
Hirnantian; Upper Ordovician; Ordovician; Paleozoic	36010010
Katian; Upper Ordovician; Ordovician; Paleozoic	36010020
Sandbian; Upper Ordovician; Ordovician; Paleozoic	36010030
Middle Ordovician; Ordovician; Paleozoic	36020000
Darriwilian; Middle Ordovician; Ordovician; Paleozoic	36020010
Dapingian; Middle Ordovician; Ordovician; Paleozoic	36020020
Lower Ordovician; Ordovician; Paleozoic	36030000
Floian; Lower Ordovician; Ordovician; Paleozoic	36030010
Tremadocian; Lower Ordovician; Ordovician; Paleozoic	36030020
Cambrian; Paleozoic	37000000
Furongian; Cambrian; Paleozoic	37010000
Age 10; Furongian; Cambrian; Paleozoic	37010010
Jiangshanian; Furongian; Cambrian; Paleozoic	37010020
Paibian; Furongian; Cambrian; Paleozoic	37010030
Epoch 3; Cambrian; Paleozoic	37020000
Guzhangian; Epoch 3; Cambrian; Paleozoic	37020010
Drumian; Epoch 3; Cambrian; Paleozoic	37020020
Age 5; Epoch 3; Cambrian; Paleozoic	37020030

Epoch 2; Cambrian; Paleozoic	37030000
Age 4; Epoch 2; Cambrian; Paleozoic	37030010
Age 3; Epoch 2; Cambrian; Paleozoic	37030020
Terreneuvian; Cambrian; Paleozoic	37040000
Age 2; Terreneuvian; Cambrian; Paleozoic	37040010
Fortunian; Terreneuvian; Cambrian; Paleozoic	37040020
Neoproterozoic	40000000
Ediacaran; Neoproterozoic	41000000
Cryogenian; Neoproterozoic	42000000
Tonian; Neoproterozoic	43000000
Mesoproterozoic	50000000
Stenian; Mesoproterozoic	51000000
Ectasian; Mesoproterozoic	52000000
Calymmian; Mesoproterozoic	53000000
Paleoproterozoic	60000000
Statherian; Paleoproterozoic	61000000
Orosirian; Paleoproterozoic	62000000
Rhyacian; Paleoproterozoic	63000000
Siderian; Paleoproterozoic	64000000
Neoarchean	70000000
Mesoarchean	80000000
Paleoarchean	90000000
Eoarchean	100000000
Hadean	110000000

Cz	Cenozoic
H	Holocene
Q	Quaternary
Ps	Pleistocene
Ng	Neogene
Pg	Paleogene
T	“Tertiary”
Pl	Pliocene
Mi	Miocene
Ol	Oligocene
Eo	Eocene
Pa	Paleocene
Mz	Mesozoic
K	Cretaceous
J	Jurassic
Tr	Triassic
Pz	Paleozoic
P	Permian
C	Carboniferous

Pe	“Pennsylvanian”
M	“Mississippian”
D	Devonian
S	Silurian
O	Ordovician
Ca	Cambrian
Pr	Proterozoic
Z	Neoproterozoic
Y	Mesoproterozoic
X	Paleoproterozoic
A	Archean

PFYC ranks Generally Assigned for Domain	Domain Choices
1	Igneous Rock
1	Metamorphic Rock
1	Precambrian Age
2	Fossils very rare
2	Recent aeolian
2	Younger than 10,000 years
2	Diagenetic alteration
3	Common invertebrate/plants intermittent
3	Significant fossils widely scattered
4	Significant fossils documented
4	Rare or uncommon fossils may be present
5	Significant fossils documented and occur regularly
6	Water
7	Ice
8	Unknown or poorly studied

Appendix B: Geologic Maps used for PFYC 'Geology Layer' feature class

Map Title	Authors	Scale	Publication Year
Preliminary Geologic Map of the Lake Mead 30' X 60' Quadrangle, Clark County, Nevada	L.S. Beard, R.E. Anderson, D.L. Block, R.G. Bohannon, R.J. Brady, S.B. Castor, E.M. Dubendorfer, J.E. Faulds, T.J. Felger, K.A. Howard, M.A. Kuntz, V.S. Williams.	1:100,000	2007
Geologic and Physical Maps of the Las Vegas 30' X 60' Quadrangle, Clark and Nye Counties, Nevada, and Inyo County, California	William R. page, Scott C. Lundstrom, Anita G. Harris, Victoria E. Langenheim, Jeremiah B. Workman, Shannon A. Mahan, James B. Paces, Gary L. Dixon, Peter D. Rowley, B.C. Burchfiel, John W. Bell, Eugene I. Smith	1:100,000	2005
Surficial Geologic Map of the Ivanpah 30' X 60' Quadrangle, San Bernardino County, California, and Clark County, Nevada	David M. Miller	1:100,000	
Geologic Map of the Pahranagat Range 30' X 60' Quadrangle, Lincold and Nye Counties, Nevada	Jayko A. S.	1:100,000	

Preliminary Geologic Map of the Pahute Mesa 30' x 60' Quadrangle, Nevada	Minor, S.A., Sawyer, D.A., Wahl, R.R., Frizzel, V.A., Schilling, S.P., Warren, R.G., Orkild, P.P., Coe, J.A., Hudson, M.R., Fleck, R.J., Lanphere, M.A., Swadley, W.C., Cole, J.C.	1:100,000	1993
Digital Geologic Map of the Nevada Test Site and Vicinity, Nye, Lincoln and Clark Counties, Nevada, and Inyo County California	Janet L. Slate, Margaret E. Barry, Peter D. Rowley, Christopher J. Fridrich, Karen S. Morgan, Jeremiah B. Workman, Owen D. Young, Gary L. Dixon, Van S. Williams, Edwin H. McKee, David A. Ponce, Thomas G. Hildenbrand, W.C. Swadley, Scott C. Lundstrom, E. Bartlett Ekren, Richard G. Warren, James C. Cole, Robert J. Fleck, Marvin A. Lanphere, David A. Sawyer, Scott A. Minor, Daniel J. Grunwald, Randell J. Laczniak, Christopher M. Menges, James C. Yount, Angela S. Jayko	1:120,000	1990
Geology and mineral deposits of Lyon,	ames G. Moore with a section on Industrial	1:250,000	1969

Douglas, and Ormsby counties, Nevada	mineral deposits, by N.L. Archbold		
Geology and mineral deposits of Washoe and Storey counties, Nevada	Harold F. Bonham, with a section on "Industrial rock and mineral deposits," by Keith G. Papke	1:250,000	1969
Geology and mineral deposits of Humboldt County, Nevada	Ronald Willden	1:250,000	1964
Geology and mineral deposits of Pershing County, Nevada	Maureen G. Johnson	1:250,000	1977
Geology and mineral resources of Elko County, Nevada	Arthur E. Granger, Mendell M. Bell, George C. Simmons, and Florence Lee	1:250,000	1957
Geology and mineral resources of Eureka County, Nevada	Ralph J. Roberts, Kathleen M. Montgomery, and Robert E. Lehner	1:250,000	1967
Geology and mineral deposits of Lander County, Nevada	John H. Stewart, Edwin H. McKee, and Harold K. Stager	1:250,000	1977
Geology and mineral resources of White Pine County, Nevada: Part I, Geology, by Richard K. Hose and M.C. Blake, Jr.; Part II, Mineral resources, by Roscoe M. Smith	Richard K. Hose, M.C. Blake, Jr., and Roscoe M. Smith	1:250,000	1976

Geology and mineral deposits of Mineral County, Nevada	Donald C. Ross	1:250,000	1961
Geology and mineral deposits of Esmeralda County, Nevada	J. P. Albers and J.H. Stewart	1:250,000	1972
Geology and mineral resources of Nye County, Nevada	Kleinhampl and Ziony	1:250,000	1985
Tectonic Map of Linclon County, Nevada	C. M. Tschanz and E. H. Pampeyan	1:250,000	1970
Preliminary surficial geologic map of Clark County, Nevada	P. Kyle House, Heather Green, Abbey Grimmer, and the Nevada Digital Dirt Mapping Team	1:150,000	2010

Appendix C: Las Vegas Formation & Laterally Equivalent Units

Geologic Map of the Corn Creek Springs Quandrangle, Nevada

Fine-grained alluvium of Tule Springs (Qts), (Qts_{1-F})

Paleospring, paludal, and fluvial deposits comprising extensive fine-grained valley-bottom fill in the upper Las Vegas Valley; related to extensive groundwater discharge during glacial/pluvial periods (Quade, 1983, 1986; Quade and others, 1995). Originally believed to be largely lacustrine in origin and mapped as the Las Vegas Formation (Longwell and others, 1965; Haynes, 1967). In the Corn Creek Springs Quadrangle, deposits are correlated with Qts in the adjacent Tule Springs Park Quadrangle (Bell and others, 1998; and divided into four members (units C, D, E, and F) after Haynes (1967) and Quade (1983).

Geologic Map of the Gass Peak SW Quadrangle, Clark County, Nevada

Fine-grained deposits of Tule Springs

Qtf: Tufa deposits, contemporaneous with Qtse

Qtse: Unit E of Haynes, 1967(includes subunits E0,E1, and E2, undivided on map)

Qtsd: Unit D of Haynes, 1967

Qtsc: Unit C of Haynes, 1967

Qtsb: Unit B of Haynes, 1967 (includes subunits B0,B1, and B2, undivided on map)

Qtsa: Unit A of Haynes, 1967

Qso: Old fine-grained spring deposits of Page et al., 2005 (middle Pleistocene)

Geologic Map of the Tule Springs Quadrangle, Nevada

Fine-Grained Alluvium of Tule Springs (Qts), (Qts_{e-c})

Spring and paludal deposits comprising of extensive fine-grained valley-bottom fill in the upper Las vegas Valley; related to extensive groundwater discharge during glacial/pluvial periods (Quade, 1983, 1886; Quade and others, 1995). Originally believed to be largely lacustrine in origin (Longwell and others, 1965; Haynes 1967) and mapped as the Las Vegas Formation by Longwell and others (1965); named the Tule Springs alloformation by Donovan (1996). Divided here into three members (units C, D, and E) after Haynes (1967).

References

Ali Baig, H, M., Zhang L., Tong, Shuai., Tong, Qingxi., 2014, Derivation of a tasseled cap transformation based on landsat 8 at-satellite reflectance,Remote Sensing Letters, vol 5, no. 5 pp. 423-431

Bonde, J.W., Varricchio, D.J., Jackson, F.D., Loope, D.B., and Shirk, A.M., 2008, Dinosaurs and Dunes! Sedimentology and paleontology of the Mesozoic in the Valley of Fire State Park, in Debendorfer, E.M. and Smith, E.I. eds., Field Guide to plutons, volcanoes, faults, reefs, dinosaurs and possible glaciation in selected areas of Arizona, California and Nevada, Geological Society of America Field Guide11, pp. 249-262

Bonde, J.W., Varricchio, D.J., Bryant, G., and Jackson, F.D., 2012, Mesozoic vertebrate paleontology of Valley of Fire State Park, Clark County, Nevada, in Bonde,J.W. and Milner, A.R.C. eds., Field Guide for the 71st annual Meeting of the Society of Vertebrate Paleontology, Paris Las Vegas, Nevada, Nevada State Museum Paleontological papers 1, pp. 108-126

Bonde, J.W., Hilton, R.P., Jackson, F.D., and Druschke, P.A., 2015, Fuana of the Newark Canyon Formation (Lower Cretaceous), east-central Nevada, Geological Society of Nevada Symposium, pp.139-150

Borak D, R., Devadiga S, W., Zheng, M., Descloitres J., 2002, The MODIS land product quality and assessment approach, Remote Sensing of Environment, 83: 62,76)

Chander, G., Markham L, B., Helder, L, D., 2009, Summary of Current Radiometric Calibration Coefficients for Landsat MSS, TM, ETM+, and EO-1 ALI Sensorsin Press, Remote Sensing of Environment, Manuscript Number; RSE-D-08-00684

Chavez Pat, S., MacKinnon David J., 1994, “Automatic Detection of Vegetation Changes in Southwestern United States Using Remotely Sensed Images”; Photogrammetric Engineering & Remote Sensing; vol. 60, no. 5; pp. 571-583

Crutchley S., 2006, Light Detection and Ranging (lidar) in the Witham Valley, Linconlshire: an assessment of New Remote Sensing Techniques, Archaeological Prospection, Archeol. Prospect. 12, 251-257.

David, L., 1941, Leptolepis nevadensis, a new Cretaceous fish, Journal of Pelontology, v. 15, pp. 318-321

English, A.M., and Babcock, L.E., 2010, Census of the Indian Springs lagerstatte, Poleta Formation (Cambrian), western Nevada, USA, Paleogeography, Paleoclimatology, Paleoecology, v. 295, pp. 236-244

Firl, G.J., and Carter, L., 2011, Lesson 10: Calculating Vegetation Indices from Landsat 5TM and Landsat 7ETM+ Data, Colorado State University Lecture

Frey, W, H., 2012, Population Growth in Metro America since 1980: Putting the Vilatile 2000’s in perspective, Washington D.C., Brookings, Print

Hardy, F.C., Bonde, J.W., 2015, Stomping around the Sump: Miocene pygmy gomphothere from Esmeralda County, Nevada, Geological Society of Nevada Symposium, pp. 923-937

Haynes, Jr., V, C, 1965 Quaternary Geology of the Tule Springs Area, Clark County Nevada, ProQuest Dissertations and Thesis; University of Arizona, Department of Geology.

Hopkin, E.K., and McRobers, C.A., 2005, A new middle Triassic flat clam (Pterioida: Halobiidae) from the middle Anisian of north-central Nevada, USA, Journal of Paleontology, v. 79, pp. 796-800

Howarth J, P., Wickwarge, M., 1999, Procedure for Change detection using Landsat Digital Data, International Journal of Remote Sensing; vol. 20, no. 1, 139-152

Huang, C., Wylie B, K., Yang, L., Homer, C., Zylstra, G., Derivation of a Tasseled Cap Transformation Based on Landsat 7 At-Satellite Reflectance, (2002), Publications of the US Geological Survey, 110

Huete A, R., "Soil Adjusted Vegetation Index (SAVI)"; 1988 Remote Sensing of Environment vol. 25; pp. 298-309

Khanna, S., Palacious-Orueta, A., Whiting, M.L., Ustin, S.L., Riano, D., Litago, J., 2007, Development of angle indexes for soil moisture elimination, dry matter detection and land-cover discrimination, Remote Sensing of Environment, v. 109, pp. 154-165

Kotz, D.M., 2009, The Financial and Economic Crisis of 2008: A systematic crisis of neoliberal capitalism, Review of Radical Political Economies, V 41. No. 3, pp. 305-317

Ligget, G. 2015, Bureau of Land Management, Official Bureau of Land Management Potential Fossil Yield Classification for the Geologic Formations of Montana, North Dakota, and South Dakota, version 9/15/2015: Billings, Montana, Bureau of Land Management, p 1-97.)

Longley A. P., Goodchild F. P, Maguire J. D., Rhind W. D., (2015). Geographic Information Science and Systems, (4th Ed). 1.1.1)

Longwell, C., E. H., Pampeyan, B, Bower, Roberts R, J., 1965, Geology and Mineral Deposits of Clark County, Nevada. Nevada Bureau of Mines and Geology, Bulletin 62, xxx p.

MacNeil, F.S., 1939, Fresh-water invertebrates and land plants of Cretaceous age from Eureka, Nevada, Journal of Paleontology, v. 13, pp. 355-360

Markham, B., L, Chander, G., Summary of Current Radiometric Calibration Coefficients for Landsat MSS, TM, TM+ and EO-1 ALI Sensors 2009, in Press, Remote Sensing of Environment, Mauscript Number; RSE-D-08-00684

Mas F, J., 1999, Monitoring land-cover changes: a comparison of change detection techniques, Int. J. of Remote Sensing vol 20, no 1, 139-152

Murphy, M.A., Morgan, T.G., and Dineley, D.L., 1976, Astrolepis sp. From the Upper Devonian of central Nevada, Journal of Paleontology, v. 50, pp. 467-471

Quade, J., 1985, Late Quaternary Environmental Changes in the Upper Las Vegas Valley, Nevada. Quaternary Research 340-357

Ramelli, R. A., Page, R, W., Manker R, C., Springer, B, K., 2011, Geologic Map of the Gass Peak SW Quadrangle, Clark County, Nevada, Nevada Bureau of Mines and Geology, Open File Report 175

Rech, A, J., Springer, K., Pigati, S. J., 2017, The Great Acceleration and the Disappearing Surficial Geologic Record, GSA Today, vol 28

Research Division, Nevada Legislative Counsel Bureau, Public Lands and General Natural Resource Issues, Policy and Program Report, April 2016

Richards, John A., 2013, Remote Sensing Digital Image Analysis, New York: Springer Heidelberg, 37-43; ch.2.

Rowland M, S., Bonde W, J., 2015, Paleontology and paleoclimatology of Tule Springs Fossil Beds National Monument and adjacent Nevada State Parks land,Department of Geoscience, University of Nevada Las Vegas

Rowland M, S., Breithaupt H. B., Stoller M. H., Matthews A. N., Saines M., 2014, First Report of Dinosaur, Synapsid and rthropod tracks in the Aztec Sandstone (Lower-Middle Jurassic) of Red Rock Canyon National Conservation Area, Southern Nevada. Fossil Footprints of Western North America, New Mexico Museum of Natural History, 62, pp 249-259

Rowland, S.M., Mercadante, M. J., 2014, Trackways of a Gregarious, Dunefiled-Dwelling, Early Jurassic Therapsid in the Aztec Sandstone of Southern Nevada, Society for Sedimentary Geology, vol 29, no 10, pp. 539-552

Rowland, S.M., Oliver, L.K., and Hicks, M., 2008, Ediacaran and early Cambrian reefs of Esmeralda County, Nevada: Non-congruent communities within congruent ecosystems across the Neoproterozoic-Paleozoic boundary, Geological Society of America Field Guide 11, pp. 83-100

Scott, E., Springer, B. K., Sagebiel, C. J., 2017, The Tule Springs Local Fauna: Rancholabrean Vertebrates From the Las Vegas Formation, Nevada, vol 443, Part A, pp. 105-121

Schowengert, R, A., 1997, “Techniques of Image Processing and Classification in Remote Sensing”, New York: Academic Press

Singh A, Digital Change detection techniques using remotely-sensed data, Int. J. Remote Sensing, vol 10, no 6, 989-1003

Springer, B. K., Pigati, S. J., Scott, E., 2017, Vertebrate Paleontology, Stratigraphy and Paleohydrology of Tule Springs Fossil Beds National Monument, Nevada (USA), Geology of the Intermountain West, vol 4, 55-98

Stidham, T.A., and Stidham, J.A., 2000, A new Miocene band-winged grasshopper (Orthoptera Acrididae) from Nevada, Annals of the Entomological Society of America, v. 93, pp. 405-407

Stoller, M. H., Rowland, M. S., Jackson, D. F., 2013, Dinosaur and Arthropod Tracks in the Aztec Sandstone of Valley of Fire State Park, Nevada. Publisher: California State University Desert Symposium, pp 159 164

Swartz, B., 2012, A marine stem-tetrapod from the Devonian of western Nevada, North America, PlosONE, v. 7, e33683

Vogelmann, J, E., Helder, D., Morfitt, R., Choate, M, J., Merchant, J, W., 2001, Effects of Landsat 5 Thematic Mapper and Landsat 7 Enhanced Thematic Mapper Plus radiometric and geometric calibrations and corrections on landscape characterization, USGS Staff- Published Research Paper 527

Yuan Fei, Bauer, E, Marvin., "Comparison of impervious surface area and normalized difference vegetation index as indicators of surface heat island effects in Landsat imagery"; Remote Sensing of Environment; vol.106, 2007; pp. 375-386

Zhang Q, Wang J, Peng X, Gong P, Shi P., 2002, Urban built-up land change detection with road density and spectral information for multi-temporal Landsat TM data, International Journal of Remote Sensing, vol 23, no. 15, pp. 3057-3078

Curriculum Vitae

John Jayson Medema

geomedema81@gmail.com

Education:

M.S., GIS, Remote Sensing, University of Nevada, Las Vegas Spring
May 2019

B.S., Geology, University of Nevada, Las Vegas
Spring 2015

Experience:

Geographic Information Systems (GIS) Specialist – Southwest Gas Corp. April 2019-present

- Natural Gas mapping specialist
- Construction As-built Quality Analyst

Geographic Information Systems (GIS) Technician – Sunrise Engineering

September 2017-April 2019

- Natural Gas mapping specialist
- Construction As-built Quality Analyst

Graduate Teaching Assistant –University of Nevada Las Vegas, department of Geoscience

- Geology 430/620 –Geographic Information Systems Applications
- Lab instructor
- Capstone project consultant

Bureau of Land Management, Department of Interior September 2016-May 2017

- Construction of geodatabase for state-wide survey of Paleontological resources
- Digitizing published geologic maps
- Construction and population of robust attribute tables meeting BLM project specifications
- Literature review justification of potential fossil yield classification (PYFC) for all surficial geologic units

Quantum Spatial-Hyperspectral Remote Sensing Technician July 2015 –July 2016

- Training manager for Vegetation Health Risk analysis -CEMA 2015
- Vegetation Health Risk lead for T-LINES Phase 2 Project
- Health Risk workflow quality control lead
- Research and Development of ATCOR Radiometric processing of Hyperspectral Imagery
- LiDAR Ground Editing workflow distribution and quality control
- Geodatabase management
- Hyperspectral Tree Species Classification
- Hyperspectral Imagery processing, CASI and HEADWALL instruments
- LiDAR ground modeling, point classification, feature extraction
- Microstation 3-D infrastructure modeling

Research Assistant with Desert Research Institute 2013-2015 and 2016-2017

- Multi-year remote sensing project using Moderate Resolution Imaging Spectroradiometer (MODIS) and Landsat satellite data to study vegetation and evapotranspiration indexes for Southern Nevada Water Authority (SNWA) at selected sites in east central Nevada
- Structure from motion modeling, data analytics
- Statistical analysis
- Landsat data atmospheric correction using the empirical line method (regression analysis) and ENVI advanced atmospheric correction algorithms
- Landsat 8 instrument calibration and radiance conversion
- VNIR UAS imagery analysis and canopy segmentation processing to assess climate impacts on plant cover
- UAS Image analysis of agriculture crop health and invasive species analysis
- Satellite Imagery soil study and wildfire impact analysis

Student GIS Technician-University of Nevada Las Vegas
Fall 2014

- High resolution Geographic Information System (GIS) map of asbestos occurrences. Published by Geological Society of America
- Link to published paper: http://geology.geoscienceworld.org/content/43/1/63.full?ijkey=zKWR0L7Tcx2w6&keytype=ref&siteid=gsgeology

Research Assistant-University of Nevada Las Vegas
January-May 2014

- Cross-calibration of Thermal Imaging Multispectral Scanner (TIMS) and Advanced Space borne Thermal Emission and Reflection Radiometer (ASTER) satellite data focusing on thermal wavelengths
- Development of TIMS atmospheric correction algorithm
- Created multiple high-resolution land surface emissivity maps
- ASTER derived surface albedo analysis of Alti-Plano Chile
- High resolution ASTER thermal infrared image mosaics for Alti-Plano Chile, Grand Canyon USA, Las Vegas NV, and Phoenix AZ

Geomorphology Lab Assistant-University of Nevada, Las Vegas
January-May 2014

- Geology 333; Geomorphology Lab assistant to graduate teaching assistant

Volunteer Experience

American Association of Petroleum Geologists (AAPG –UNLV Chapter.)
Spring 2017

- LiDAR short course instructor

Paleontology Field Volunteer-University of Nevada Las Vegas
Spring 2013

- Exploration of newly discovered cave systems to collect Holocene animal fossils in Parashant National Monument, AZ

Technical skills

- Remote Sensing and GIS software
  - ENVI classic, ENVI 4.8-5.1
  - ARC GIS
  - Google Earth
  - JMARS/JEARTH remotely sensed data analysis
  - Agisoft Photoscan, photogrammetry –structure from motion processing
  - ApplicationMaster (Orthorectification and Imagery Mosaic)
  - Ultramap (Radiometric correction)
  - Global Mapper (DEM allocation and modification)
  - ITRES (casi1500 hyperspectral camera image processing)
  - Davinci (script-based image processing)
  - ATCOR (atmospheric correction/image processing)

Software programs

- ENVI
- ESRI Arc GIS
- Schnieder Electric; ArcFM, Geometric Network Analysis
- Agisoft Photoscan
- PixelWrench
- SigmaPlot
- MATLAB
- ITRES
- ATCOR
- UltraMap
- Application Master (Ultracam Orthorectification/Image Mosaic processing suite)
- Microstation
- Microsoft Office
- Google Sheets
- Adobe (photoshop/illustrator)
- DAVINCI
- Minitab

Presentations:

- 2014 Geosymposium, University of Nevada Las Vegas
  Poster: Cross Calibration of TIMS and ASTER, Multi-Resolution Spectral Observations
- 2015 Geosymposium, University of Nevada Las Vegas
  Poster: Mapping Potential Mineral Hazards Using ASTER Emissivity Imagery
- 2015 Geosymposium, University of Nevada Las Vegas
  Poster: Applications of Passive Wet Screen Techniques to Site 5 Samples Collected from Valley of Fire

  2015 Geosymposium, University of Nevada Las Vegas

  Oral Presentation: Mapping Potential Mineral Hazards Using ASTER Emissivity Imagery

Programming:

- Davinci (C-based data processing)
- MATLAB
- Python (certification in process)
- ArcPy (python)

Remote sensing science applications:

- LiDAR data collection and analysis using ENVI
- LiDAR point cloud classification/infrastructure modeling/feature extraction
- Predictive Analytics
- Utility infrastructure/vegetation management
- Radiometric calibration of satellite, aerial and UAS imagery
- Vegetation Index analysis, satellite, aerial and UAS based imagery
- Canopy segmentation analysis of Tetracam Inc ADC images acquired with UAS
- High-resolution land surface temperature and emissivity mapping using ASTER
- C-based data processing of ASTER and TIMS data including instrument noise correction and atmospheric correction
- Cross-calibration of TIMS and ASTER hyper-spectral instruments
- C-based data processing to create enhanced high-resolution multi-image mosaic maps
- Ortho-rectification of satellite/aerial Imagery
- Hyperspectral principle component analysis
- Multispectral soil analysis
- UAS based agriculture crop management/analysis

References

Dr. Lynn Fenstermaker
Associate Research Professor and Deputy Director
Division of Earth and Ecosystem Sciences
NASA EPSCoR and Space Grant Director
Desert Research Institute
755 East Flamingo Rd. Las Vegas NV, 89119
Las Vegas Campus, 702-862-5412; Lynn.Fenstermaker@dri.edu

Dr. Scott Nowicki
Quantum Spatial
Remote Sensing Scientist
421 SW 6th Ave, Suite 800
Portland, OR 97204
503-662-7168; snowicki@quantumspatial.com

Dr. Josh Bonde
Assistant Professor in Residence
Taphonomy/Vertebrate Paleontology
UNLV Department of Geoscience
4505 S. Maryland Pkwy
Las Vegas NV, 89109
702-895-1774; Joshua.bonde@unlv.edu

Dr. Wanda J. Taylor
Professor of Geoscience
Structural Geology, Tectonics and Neotectonics
UNLV Department of Geoscience
4505 S. Maryland Pkwy
Las Vegas NV, 89109
702-895-4615; wanda.taylor@unlv.edu